MODEL BASED EXPLORATION OF A NEW COOLING CONCEPT

Undergraduate Honor Research Thesis

Presented in Partial Fulfillment of the Requirements for Graduation with Honor Research Distinction at The Ohio State University

By ZhaoJi Wu

Department of Mechanical and Aerospace Engineering

The Ohio State University

Columbus, OH, 43210, USA

Advisor: Dr. Sandip Mazumder

Defense Committee:

Dr. Sandip Mazumder, Advisor

Dr. Clarissa Belloni

April 2020

Abstract

Thermal management is key to the proper functioning of any engineering devices. Battery packs used in hybrid-electric vehicles need to adhere to certain temperature limits as does chips packaged within computers. Heat is the byproduct of any process, and therefore, any engineering device dissipates a lot of heat, which results in local regions of high temperature (or hot spots) within the device. Aside from lowering the peak temperature, another important consideration is the location of the hot spot. If the hot spot resides at a particular location over a long period of time, that region is prone to damage. In this research, a new cooling concept is explored. Rather than using steady coolant flow, as is traditionally done, oscillating (reversing) flow is used. In the first phase of the research, how the flow may be reversed is investigated using a Computational Fluid Dynamics (CFD) study of a fluidic oscillator. A fluidic oscillator is a device that is capable of reversing flow due to fluid instability. In the second phase, Computational Fluid Dynamics and Heat Transfer (CFD/CHT) analysis is conducted using oscillatory flow conditions to investigate if the proposed new concept has merit from a scientific standpoint. The second research phase also sheds light on the question as to what operating conditions should be used for the application in question.

Overall, two-dimensional fluidic oscillator model results in some differences between the simulation and the experimental results. Yet, the qualitative trend of the results agreed with the experimental observations. As the inlet velocity increases, the oscillating frequency of the sweeping jet increases linearly and then exhibits a nonlinear trend. Various models prove the oscillatory flow provides lower average temperature of the target body, and more uniform temperature distribution throughout the system, along with the maximum temperature point (or hot spot) in a system constantly shifts when cooling with oscillatory flow.

Acknowledgements

I would like to thank my research advisor, Dr. Sandip Mazumder. Without his continuous support, this thesis could not have been written. I would also like to thank Dr. Clarissa Belloni, who spent her time attending my thesis defense, along with fellow students, Navni Verma, Shashank Terala, and Arif Hossain, who assisted me during this research. A special thanks to the Undergraduate Honors Committee in the College of Engineering for supporting my research with the Undergraduate Research scholarship award, along with my family and friends for their support and love through this journey.

Table of Contents

List of Figures

List of Tables

Nomenclature

Abbreviations

2D	Two-dimensional
3D	Three-dimensional
CFD	Computational Fluid Dynamics
CHT	Computational Heat Transfer

Letter

A	Cross-section area of the fluidic oscillator (m^2),
B	Body force vector ($\frac{m}{s^2}$)
C_p	Specific heat ($\frac{J}{kg \cdot K}$)
D	Hydraulic Diameter
$D_{h_{2D}}$	Hydraulic diameter in 2D model (m)
$D_{h_{3D}}$	Hydraulic diameter in 3D model (m)
H	Throat height of fluidic oscillator (m)
h	Specific enthalpy ($\frac{J}{kg}$)
k	Thermal conductivity ($\frac{W}{m*K}$)
$\dot{m}$	Mass flow rate ($\frac{kg}{s}$)
P	Wetted perimeter (m)
p	Pressure (Pa)
$\dot{Q_{gen}}$	Volumetric heat generation rate ($\frac{W}{m^3}$)
Re	Reynolds number

T	Temperature (K)
t	Time (s)
U	Velocity vector ($\frac{m}{s}$)
u	Flow velocity ($\frac{m}{s}$)
V	Volume (m^3)
W	Throat width of fluidic oscillator (m)

Greek

ρ	Density ($\frac{kg}{m^3}$)
ρ_{air}	Density of air ($\frac{kg}{m^3}$)
τ	Shear stress tensor (Pa)
μ_{air}	Dynamic viscosity of the air ($\frac{kg}{m \cdot s}$)

Chapter 1: Introduction

1.1 Background and Motivation

Heat is a byproduct of any power conversion process. Inside any power conversion device, dissipated heat tends to create regions of high temperature (or hot spots). If a hot spot stays at a certain location over a long period of time, that region is prone to damage. Therefore, thermal management is key to the proper functioning of many devices both from the standpoint of maintaining an average temperature, as well as for controlling hot spots.

Most current cooling system designs have a common disadvantage or limitation. For example, cooling of battery packs in electric vehicles is currently attained by placing the battery pack on a light-weight metallic (typically aluminum) block and by running coolants through passages that are carved within the metallic block, as shown schematically in Figure 1-1. Typically, a single serpentine passage is used, although other configurations have also been considered. The primary disadvantage of such an approach is that as the coolant moves through the passages, it heats up to a temperature very close to that of the metallic block that it is trying to remove heat from. As a result, the cooling capacity is insignificant near the downstream portion of the coolant passages. Another problem with this approach is that the hot spot stays confined to a small region over an extended period of time, e.g., in this particular example, the top right corner. A stationary hot spot is dangerous and can lead to complete failure. For example, in a battery pack, if the hot spot is always confined to one or few cells in the corner, those cells may ultimately fail, and that would lead to the entire battery pack being shorted since the cells are usually placed in series. Similar events occur in solar panels, wherein failure of a single cell may cause shutdown of the entire panel. The problem can be mitigated only by

increasing the coolant flow rate. However, this would require a larger compressor/pump, which lead to additional challenges, such as:

(1) additional weight of the vehicle.

(2) additional power consumption affecting the endurance/mileage of the vehicle.

(3) additional noise production and vibrations affecting the vehicle stability and passenger comfort.

Therefore, an alternative cooling strategy is warranted.

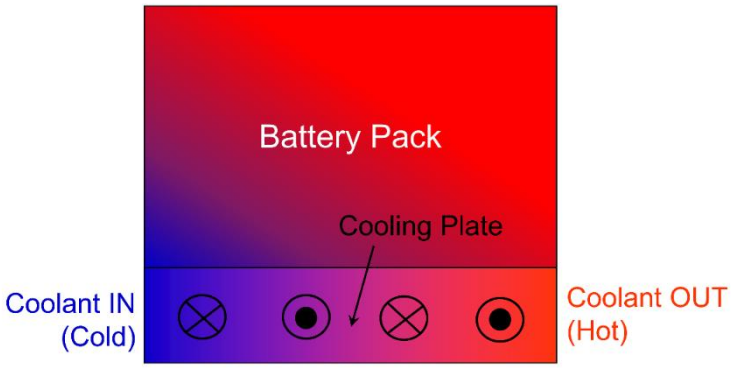

Figure 1-1: Schematic of current cooling strategy used for battery packs in electric vehicles

1.2 Problem Definition and Significance

To resolve the challenges mentioned previously, the employment of unsteady circulation of the coolant is proposed. The flow direction of the coolant reverses periodically at a frequency that optimizes cooling performance. In other words, the leftmost inlet port shown in Figure 1-1 sometimes serves as an inlet and sometimes as an outlet. Flow reversal has three potential advantages:

(1) The original downstream end of the flow passage, which suffers from "diminishing return" due to low temperature difference, now periodically encounters high temperature difference (when it becomes the upstream end or inlet of the channel).

(2) Unsteady motion of the fluid within the coolant channel could create secondary vortices that enhance heat transfer due to large-scale mixing (as opposed to parallel steady flow past channel walls) [1-5].

(3) Since the flow is unsteady, during some periods of time larger coolant flow rates may be used than others, so that the average flow rate is the same as the baseline case. However, larger flow rates (locally in time) has the potential to generate larger cooling rates, so the location of the hot spot within a system may constantly shift due to the oscillatory flow.

A schematic of the proposed concept is shown in Figure 1-2.

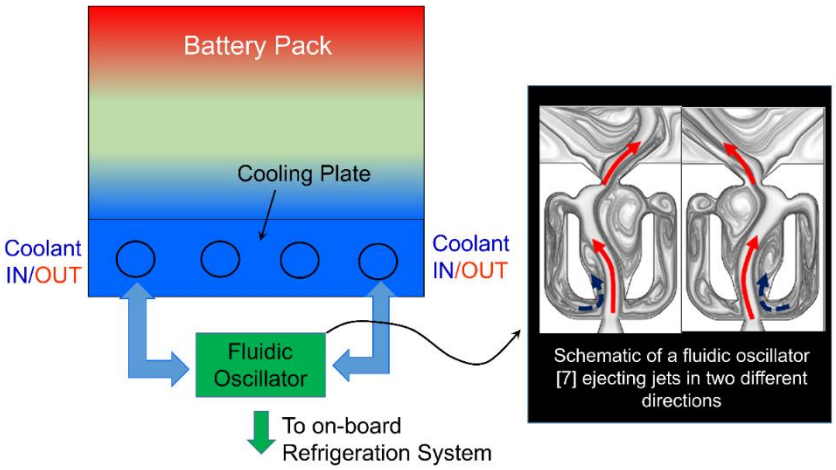

Figure 1-2: Schematic of the proposed cooling strategy for battery packs in electric vehicles

The flow reversal (oscillation) may be achieved using a fluidic oscillator [6,7], which is a hydraulically actuated device that changes flow direction without additional moving parts. The working principle of a fluidic oscillator is illustrated in Figure 1-2. A jet enters and fills the cavity and the feedback channels, forming two opposite vortices on both sides of the jet. As the intensity of the vortices increases, one vortex becomes dominant, causing the jet to deflect against the wall. This enables fluid enter the feedback loop which flows back and causes the jet switches to the opposite wall and the same process repeats, resulting in an oscillatory fluid

motion [7]. It has been used successfully in the gas turbine industry for film cooling applications. A CFD study is first conducted to validate the model of this device and optimize the performance of this device. Following this CFD study, computational heat transfer analysis is conducted to understand the effect of oscillating flow on heat transfer.

1.3 Objectives

The objectives of this research are divided into three major parts:

(1) Part I: Conduct CFD studies to optimize the size and operating conditions of the fluidic oscillator that is used to reverse the flow.

(2) Part II: Conduct preliminary CFD/CHT analysis to explore the effect of oscillatory flow on cooling.

(3) Part III: Optimization of the entire cooling concept via CFD/CHT simulation and demonstrate its effectiveness for a particular application.

Chapter 2: Research Method

2.1 Simulation Software and Governing Equations

A commercial computational fluid dynamics (CFD) software program, ANSYS-Fluent™ is used to conduct coupled fluid flow and thermal analysis. The simulations include compressible fluid flow, and heat transfer by conduction and convection, including conjugate heat transfer. The governing equations of compressible fluid flow and heat transfer, expressed in vector form are [8]:

Conservation of mass:

$$\frac{\partial \rho}{\partial t} + \nabla \cdot (\rho U) = 0 \tag{2.1}$$

Conservation of momentum:

$$\frac{\partial}{\partial t}(\rho U) + \nabla \cdot (\rho U U) = -\nabla p + \nabla \cdot \tau + \rho B \tag{2.2}$$

Conservation of energy:

$$\frac{\partial}{\partial t}(\rho h) + \nabla \cdot (\rho U h) = \nabla \cdot (k \nabla T) + \dot{Q_{gen}} \tag{2.3}$$

where B is the body force vector ($\frac{m}{s^2}$), h is the specific enthalpy ($\frac{J}{kg}$), k is the thermal conductivity ($\frac{W}{m*K}$), p is the pressure (Pa), $\dot{Q_{gen}}$ is the volumetric heat generation rate ($\frac{W}{m^3}$), T is the temperature (K), U is the velocity vector ($\frac{m}{s}$), ρ is the density ($\frac{kg}{m^3}$), τ is the shear stress tensor (Pa). The conservation of mass and moment equations are applied in both compressible fluid flow and heat transfer simulations. The conservation of energy is applied in the heat transfer simulations.

2.2 CFD Study of the Fluidic Oscillator

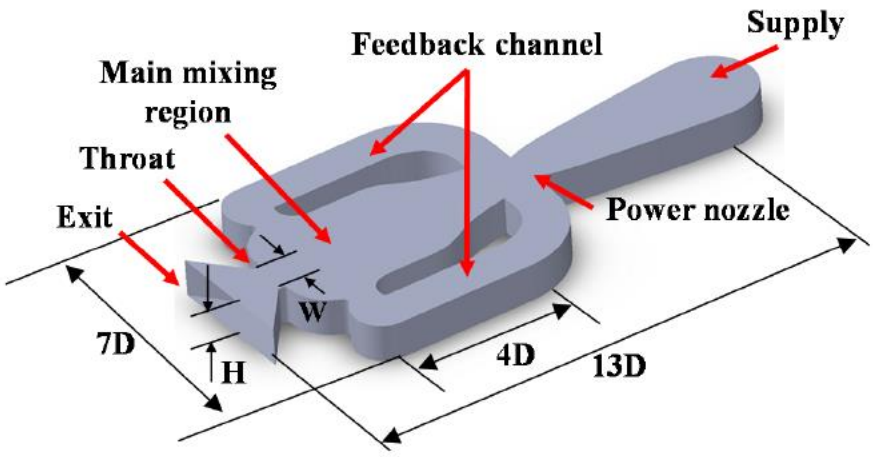

Figure 2-1: 3D fluidic oscillator model (D = 4.1 mm) [7]

2.2.1 Model Description

The 3D model of the fluidic oscillator [7] was obtained from the Ohio State University researcher, Mohammad A. Hossain [7]. The model is shown in Figure 2-1, with height H, width W, and hydraulic diameter D are all 4.1 mm [7]. The hydraulic diameter is based on the throat cross section. A 2D surface model is extracted from the 3D model with the same dimension, and an extended domain is created (see Figure 2-2) so that appropriate boundary conditions can be set at the outlet. The length of the extended domain is 60D and the width is 48D.

2.2.2 Validation

Calculations were conducted using the 2D model, and the results are validated against the experimental data from Hossain[7] by running series of simulations with the same inlet conditions listed in the experimental dataset and comparing simulated oscillation frequency of the sweeping jet with the experimental results. Table 2-1 shows the experimental data. The mass flow rate has been converted to inlet velocity based on Reynolds number (see Appendix section 1 for a sample conversion).

Table 2-1: Experimental data of the fluidic oscillator [7]

Mass flow rate (g/s)	Reynolds Number	Velocity inlet speed (m/s)	Measured Oscillation Frequency (Hz)
0.79	4699	2.3364	146
1.18	7019	3.4898	210
1.58	9398	4.6727	284
1.97	11718	5.8261	352
2.37	14098	7.0091	414
2.76	16417	8.1625	466
3.16	18797	9.3455	514
3.55	21117	10.4989	560
3.95	23496	11.6819	605
4.34	25816	12.8353	644
4.74	28195	14.0182	680
5.13	30515	15.1716	684

2.2.3 Simulation Setup

The full simulation domain and its boundary conditions are presented in Figure 2-2. The domain's rightmost end is set as a pressure outlet with 0 gage pressure. The upper, lower, and left ends of the domain is set to symmetry boundary condition. The surfaces of the fluidic oscillator are set as smooth walls, and the inlet of the fluidic oscillator is set as a constant velocity inlet. Interior lines of the extended domain separate regions with different cell sizes, which is explained later in this section. The working fluid inside of the fluidic oscillator is air at sea-level, 20 °C condition, consistent with Hossain's experiment setup [7]. The density of the air is $1.225\,\frac{kg}{m^3}$ and the dynamic viscosity of the air is $1.7894 \cdot 10^{-5}\,\frac{kg}{m \cdot s}$.

Since the calculated Reynolds numbers (Table 2-1) are all in the turbulent regime (> 2300), a turbulence model must be used to capture the effects of turbulence. In this particular

case, realizable $k-\epsilon$ turbulence model with curvature correction is applied, due to its low computational cost, high convergence rate, and effectiveness of simulating oscillating flow [8]. The turbulent intensity is assumed to be 5% since better estimates are not available. The SIMPLE algorithm is used for pressure-velocity coupling, and a convergence criterion for continuity, x momentum, y momentum, k, and epsilon are set to 10^{-3}. A time step size of 0.0005s is used and the total simulated flow duration is 1 second.

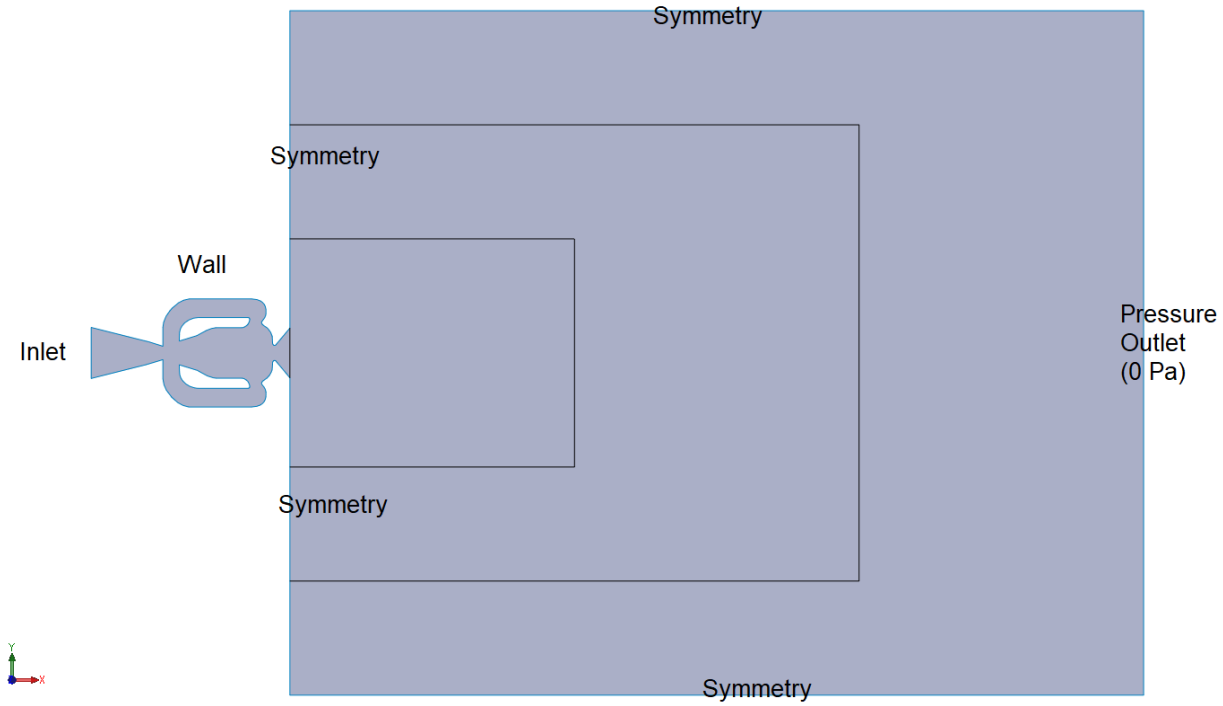

Figure 2-2: 2D fluidic oscillator model

The 2D model is meshed using the ANSYS ICEM-CFD software, and a sample mesh is illustrated in Figure 2-3. Inside of the fluidic oscillator triangular cells are used with a maximum cell size of 0.1023 mm. The maximum cell size is calculated based on using the highest inlet velocity in Table 2-1 to constraint the y^+ value to less than 11. The outside domain (to the right of the fluidic oscillator's outlet) consists of quadrilateral cells with two times the size of triangular cells inside of the fluidic oscillator, then the cell size gradually increases to reduce the

cell count, so that the computational time can be kept to a minimum. To further reduce the y^+ value near the fluidic oscillator surface, additional cell layers with size of 0.05115 mm are created, so the detail of turbulence behavior near the surface can be captured, and accuracy of the model can be improved. The detailed view of the additional layer is shown in Figure 2-4.

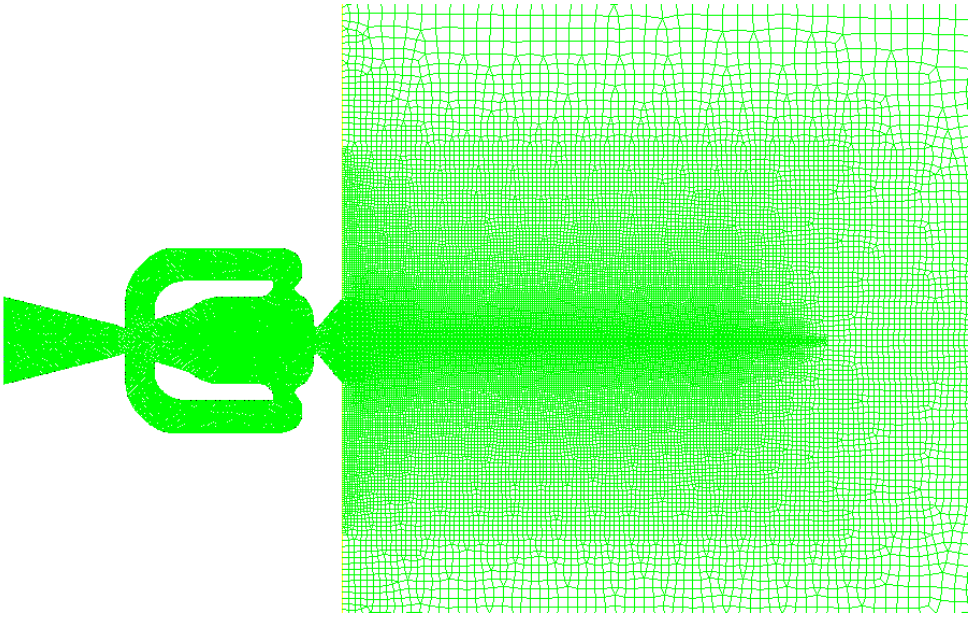

Figure 2-3: Mesh of the 2D fluidic oscillator model

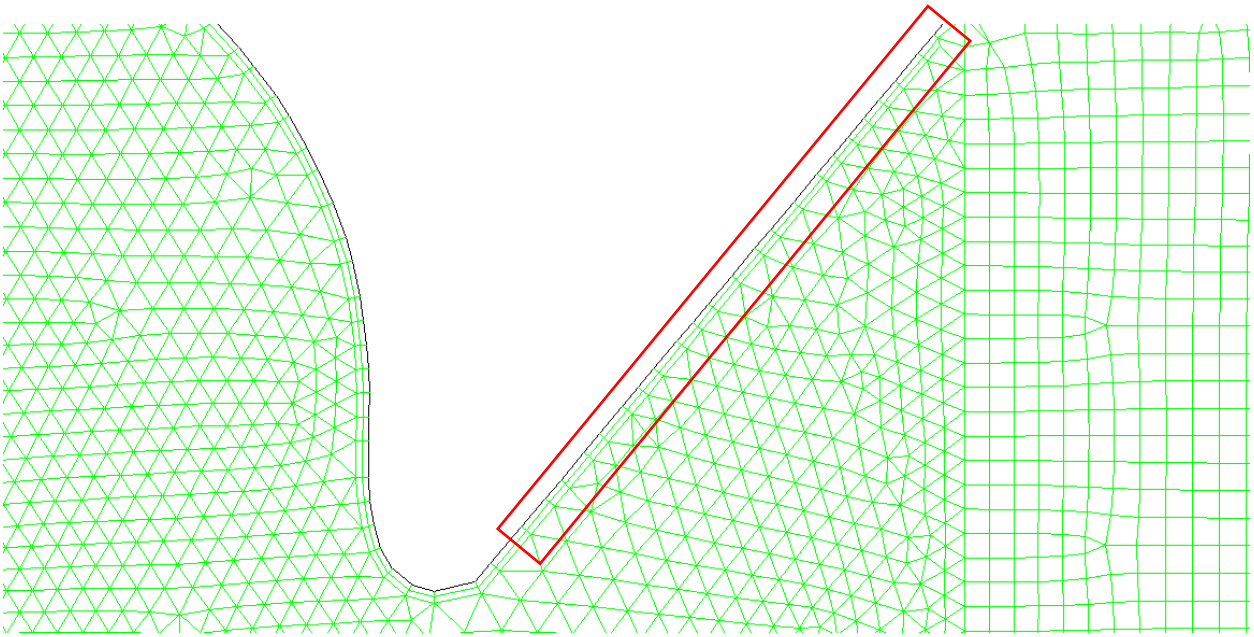

Figure 2-4: Detail view of the mesh inside the fluidic oscillator (additional layers marked in red)

2.2.4 Determining the oscillation frequency

In order to determine the oscillation frequency of the sweeping jet, two symmetrical virtual points near the outlet section of the fluidic oscillator were placed (see Figure 2-5). u-velocity of the sweeping jet passing those points during the one second duration is recorded and plotted versus time. Using Fast Fourier Transform converting the time domain data to the frequency domain, the oscillation frequency of the sweeping jet is determined.

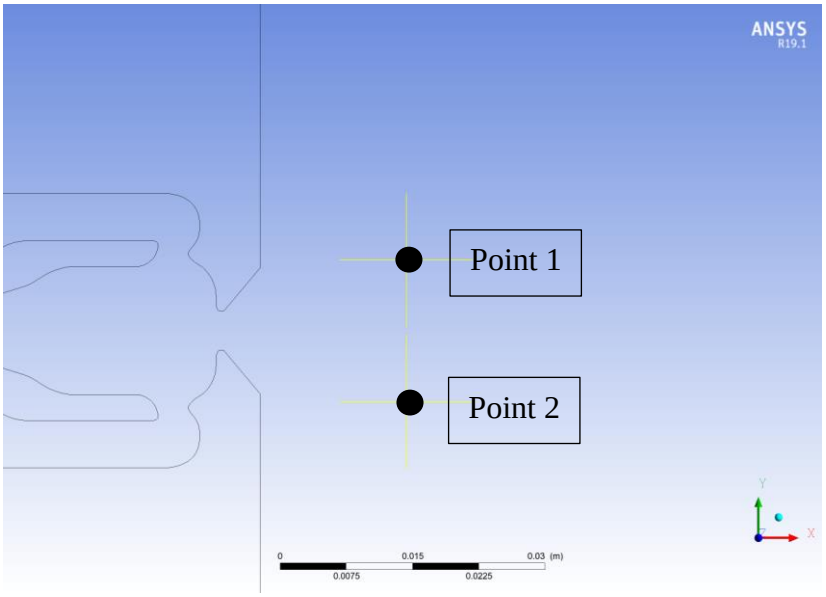

Figure 2-5: Point location for measuring oscillation frequency of the sweeping jet

2.3 CFD/CHT Investigation of Cooling with Oscillatory Flow

2.3.1 Preliminary Model Description

To study the effect of oscillatory flow on cooling, the following system is considered: a 2D system consisting of a 0.5 m x 0.5m square aluminum block with a 5 cm wide channel inside. The aluminum block is considered as the cooling plate with a heat source added to the block. The outer edges of the block are exposed to the ambient and loses heat by convection, with free stream temperature of 300 K and heat transfer coefficient of $10\,\frac{W}{m^2 \cdot K}$. The surfaces of the channel were set as smooth walls. Inlet of the channel is set as constant velocity inlet and outlet is set as

pressure outlet with gage pressure of 0 Pa. The coolant is assumed to be liquid water and enters at 20 ^{o}C. The fluid and thermal properties of water and aluminum are shown in Table 2-2.

Table 2-2: Physical properties of water and aluminum

	Liquid Water (20 °C)	Aluminum
Density ($\frac{kg}{m^3}$)	998.2	2719
Specific Heat ($\frac{J}{kg \cdot K}$)	4182	871.0
Thermal Conductivity ($\frac{W}{m \cdot K}$)	0.6	202.4
Dynamic Viscosity ($\frac{kg}{m \cdot s}$)	10^{-3}	N/A

2.3.2 Oscillatory Flow Simulation

To enable simulation of an oscillatory flow, FLUENT's built-in commands are applied (See Appendix Section 2). The commands change the boundary conditions of inlet and outlet based on the current flow time. Therefore, to simulate the change of flow direction, the original pressure outlet is set as a velocity inlet, and the original velocity inlet is set as a pressure outlet. Through changing the boundary conditions periodically, the oscillatory flow inside the channel can be simulated. Those built-in commands are applied to all the oscillatory flow simulations in the rest of models. With this approach, the velocity at each inlet is essentially constant over the period of injection.

2.3.3 Different Channel Geometry

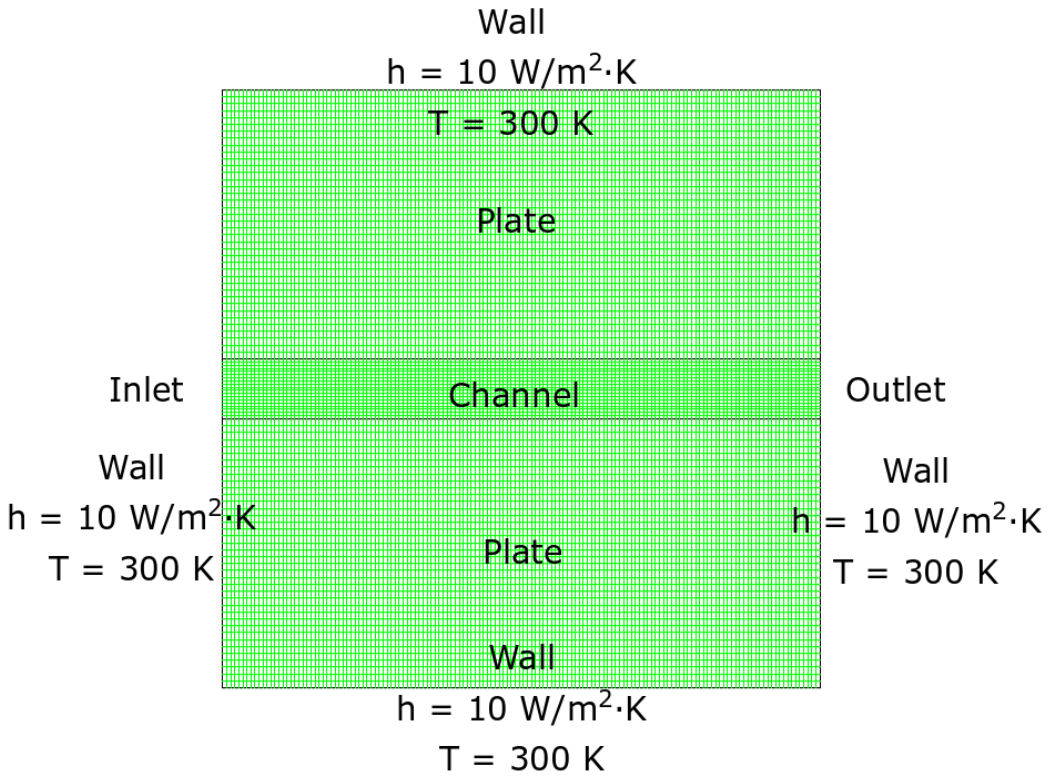

Figure 2-6: Straight channel cooling system design

The CFD/CHT study was extended to evaluating the effect of oscillatory flow in different channel geometry on cooling. Straight channel design and U-shape channel design are shown in Figures 2-6 and 2-7. Each system consists of structured quadrilateral mesh with cell size of 2.5 mm. The inlet speed is set as 0.005 m/s (Re = 500), to initially study laminar flow regimes. The oscillatory flow changes the direction every 100s as the water reaches the opposite end of the channel. The convergence criterion for continuity, x momentum, y momentum, and energy are all set to 10^{-5}. The time step size of all simulations is set as 1s, and the duration of the flow is 900s. Simulations are initialized with a temperature of 400 K everywhere in the system, and no fluid motion.

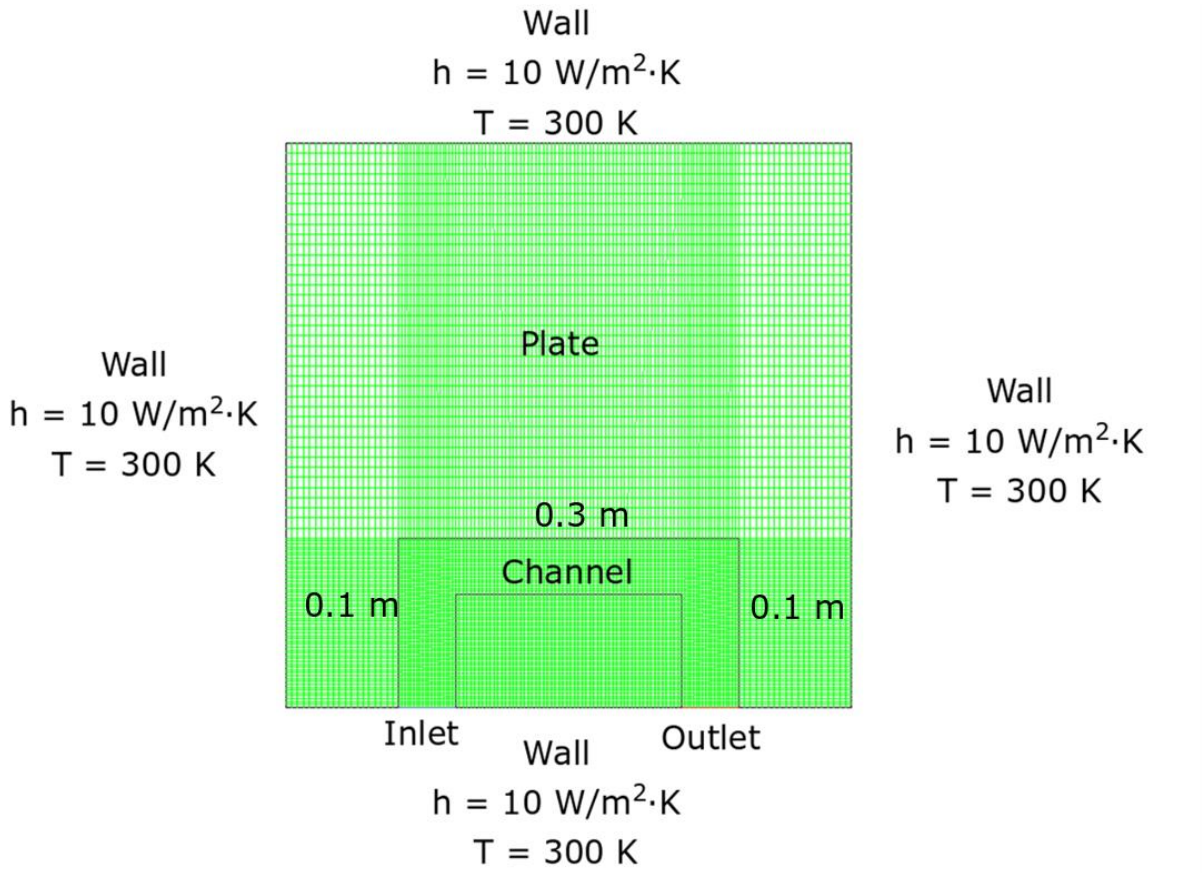

Figure 2-7: U-shape channel cooling system design

2.3.4 Quantification of Cooling Effect

To determine the effectiveness of a chosen cooling mechanism, area-weighted average temperature of the plate is computed, as follows

$$T_{avg} = \frac{\sum_{cells} T_i A_i}{\sum_{cells} A_i} \tag{2.4}$$

where T_i is the temperature of the i-th cell, and A_i is area of the cell.

By plotting the area-weighted average temperature against time, the cooling conditions that provides lower area-weighted average temperature at the end of 900 s is considered a more effective cooling system.

2.3.5 Turbulent Regime

The effect of oscillatory flow with various flow speeds is also evaluated. With the same setup, the inlet speed is changed to 0.02331 m/s, which is converted based on the lowest Reynolds number from Table 2-1 and the current system's geometry. Using the same geometry and evaluating methods mentioned previously, the effect of cooling with steady/unsteady flow in either turbulent or laminar regime is compared. In the current case, the flow changes direction once the fluid reaches the opposite end of the channel. For turbulent flow, the turbulence model being used is still the realizable $k-\epsilon$ model with curvature correction, along with the same simulation setup as in the previous model.

2.3.6 Additional Cooling System Description

Extending the U-channel design illustrated in Figure 2-7, an additional double-U channel system is also considered (see Figure 2-8). The double-U channel system penetrates deeper into the plate, and has more turns to increase the number of secondary vortices, which, as discussed earlier, may enhance heat transfer.

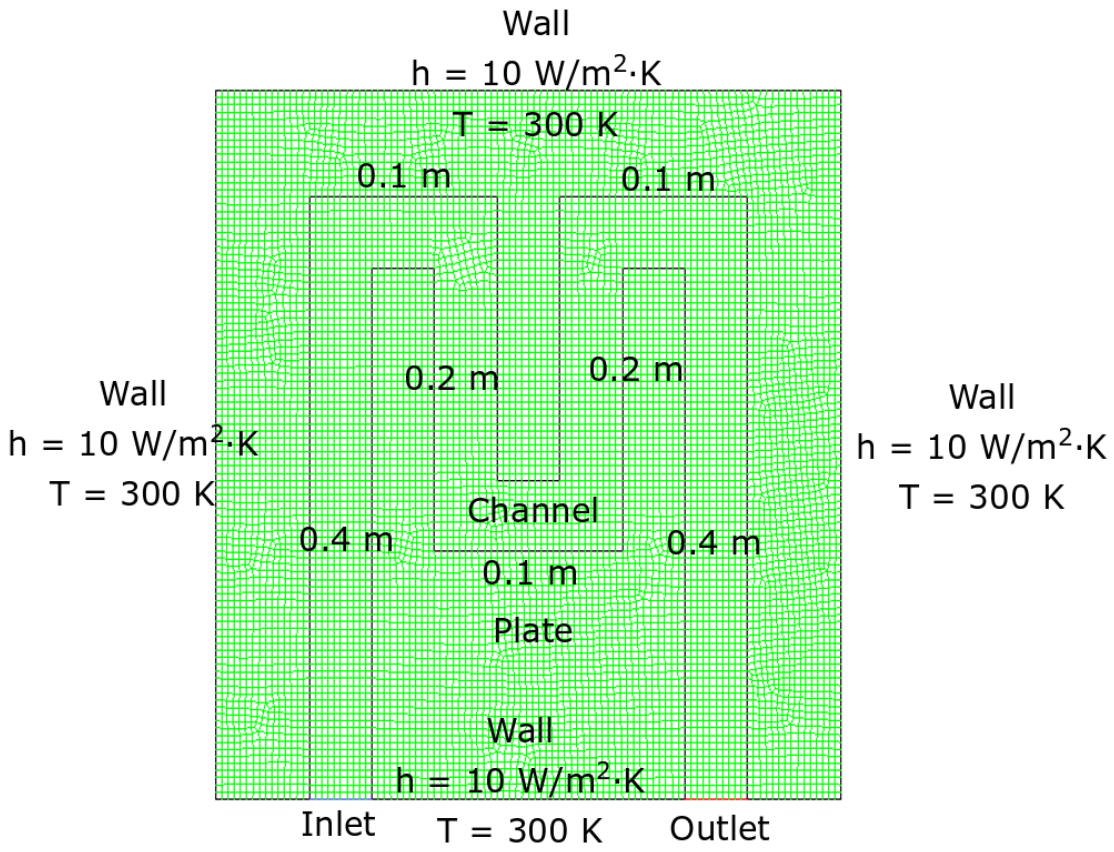

Figure 2-8: Double-U channel cooling system design

2.3.7 Effect of Oscillation Frequency

With a similar strategy, the system is tested with the inlet velocity of 0.02331 m/s (Re = 2320), but with oscillatory flow of different oscillation frequencies. The benchmark frequency in the current system is $\frac{1}{128}\ Hz$, which is calculated based on two times the exact time required for the fluid to reach the opposite end of the channel, and is considered as a full cycle for the flow direction to reverse. Then, the system is also tested with frequencies of $\frac{1}{64}\ Hz$, $\frac{1}{32}\ Hz$, $\frac{1}{256}\ Hz$, $\frac{1}{512}\ Hz$ to compare the cooling effect.

2.3.8 Cooling System Model Description for an Application

Following three preliminary investigations, a final set of simulations focused on a specific application—cooling of a battery pack—is considered. The model system is inspired by the cooling system inside Tesla's Model S (see Figure 2-9 [9]). A serpentine coolant channel is passes through the battery packs, as the water-glycol coolant flows through the channel to remove heat from battery pack

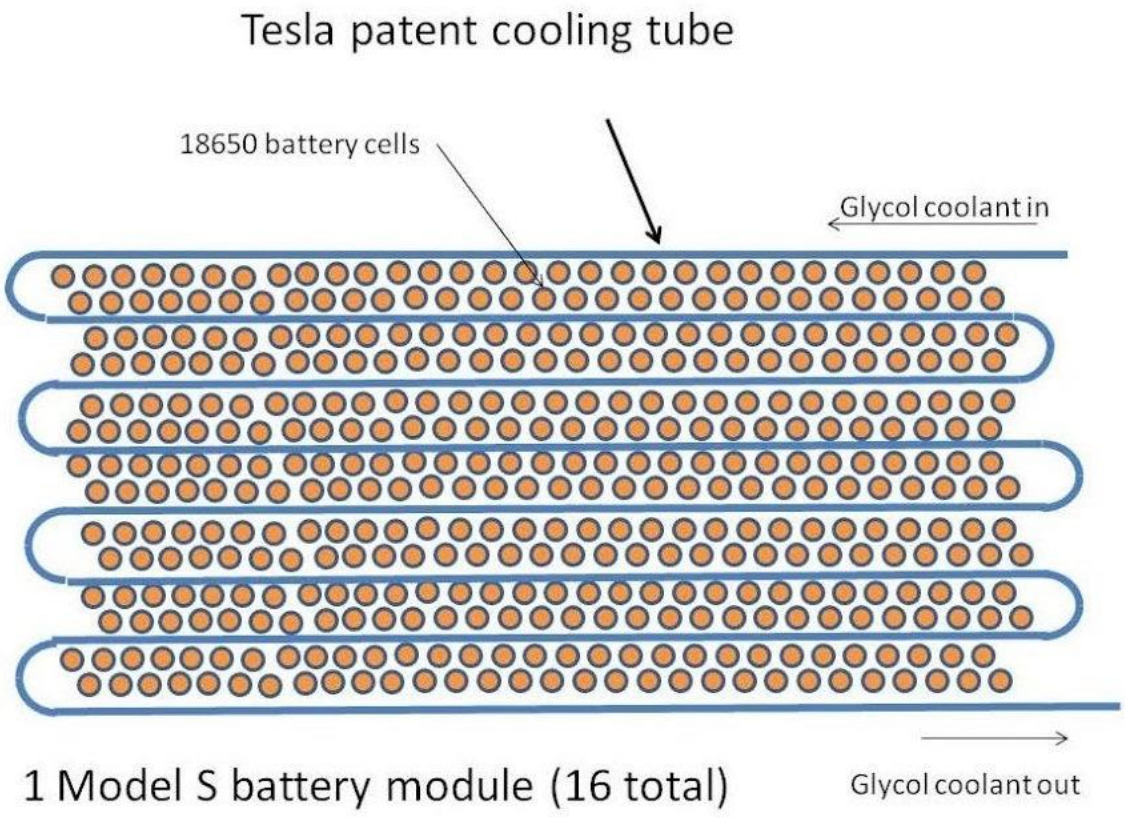

Figure 2-9: Tesla's model S cooling system design (top view)

Figure 2-10 illustrates the proposed cooling system with its corresponding boundary conditions. The inlet still serves as a velocity inlet and the outlet is a pressure outlet with 0 Pa gaga pressure. The system consists of three lithium-ion battery packs connected with a 0.5 m x 0.25 m aluminum cooling plate. There is a 5 mm channel which runs within the cooling plate alongside the battery pack. Room temperature (20 °C) liquid water is used as the coolant through the channel. Physical properties of aluminum, water, and the lithium-ion battery are shown in

Table 2-3. The density, specific heat and thermal conductivity of the lithium-ion battery are estimated from the data obtained from Wu and Lin [10-11]. Since there are multiple material layers inside the lithium-ion battery, which all have different thermal conductivity, an average value of thermal conductivity, $10\frac{W}{m\cdot K}$, is applied in this study. The heat generation rate of the battery pack is 0.2 MW/m^2 , which is assumed based on the amount of heat input required to raise the temperature of the battery by 60°C in 1000 seconds without any cooling. This is calculated using the simple energy balance:

$$\dot{Q}Vdt = \rho V C_p dT$$

$$\dot{Q} * 1000\ s = 3600\frac{kg}{m^3} * 1066\frac{J}{kg\cdot K} * 60\ °C$$

$$\dot{Q} \approx 0.2\frac{MW}{m^2}$$

where $\dot{Q}$ is volumetric heat generation rate ($\frac{MW}{m^3}$), V is Volume (m^3), dt is time interval (s), C_p is the specific heat ($\frac{J}{kg\cdot K}$), and dT is temperature change (K).

Table 2-3: Material properties in the cooling system

	Water (20 °C)	Aluminum	Lithium-ion Battery
Density ($\frac{kg}{m^3}$)	998.2	2719	3600
Specific Heat ($\frac{J}{kg\cdot K}$)	4182	871.0	1066
Thermal Conductivity ($\frac{W}{m\cdot K}$)	0.600	202.4	10
Dynamic Viscosity ($\frac{kg}{m\cdot s}$)	1.003E-3	N/A	N/A

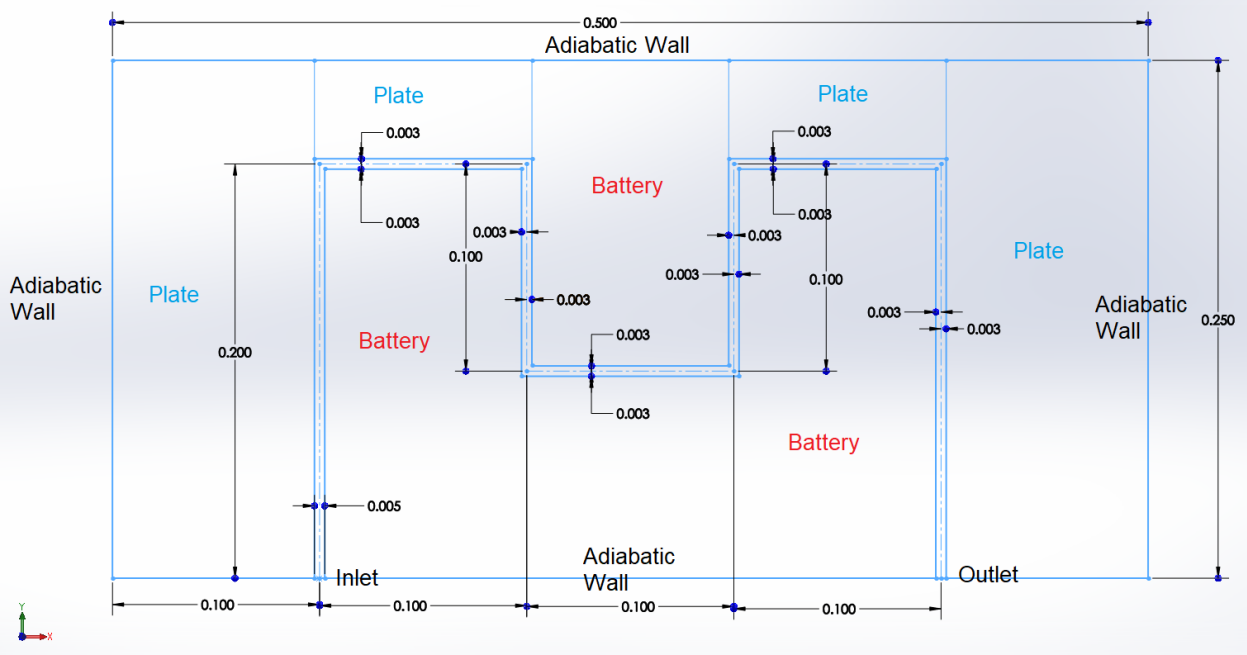

Figure 2-10: Cooling system design layout

Meshing of the system follows the same strategy as in the fluidic oscillator simulation. The 5 mm channel consists of quadrilateral and triangular cells with size of 0.1 mm, which is calculated bases on Re = 2320 and y^+ value of 11. The cell size of the plate and battery is five times the cell size inside the channel and gradually increasing towards the middle of the battery/plate in order to reduce the cell count. The detailed view of the mesh is illustrated in Figure 2-11. Once again, the realizable $k-\epsilon$ turbulent model with curvature correction is used in the simulation. The turbulent intensity at the inlet is assumed to be 5%. A convergence criterion for continuity, x momentum, y momentum, k, and ϵ are set as 10^{-3}. Time step size used in the simulation is 1s and a total duration 900 seconds is simulated. The system starts at an initial state of 293 K (20 ^{o}C), with no fluid motion.

The system is first simulated with a steady flow direction with inlet speed of 0.05 m/s, and area-weighted average temperature of the battery is recorded. Then the system is simulated with different frequency of oscillatory flows and area-weighted average temperature is again

recorded. Instead of using FLUENT's built-in commands, an oscillatory velocity profile is applied, as illustrated in Figure 2-13. The flow starts with an inlet velocity of 0.1 m/s decreasing linearly, and as the speed becomes negative, the direction of the flow reverses. The interval of 250 s is considered as a full oscillation cycle and the average flow rate in the interval is equal to 0.05 m/s, which is the same velocity used in the unidirectional simulations. To switch to different oscillation frequencies, the time interval between switching sign of the velocity is adjusted. Oscillation frequencies of $\frac{1}{40}$ Hz, $\frac{1}{80}$ Hz, $\frac{1}{160}$ Hz, $\frac{1}{320}$ Hz and $\frac{1}{640}$ Hz are explored in this study, and their cooling effect is recorded and compared with the simulation result from steady flow simulation.

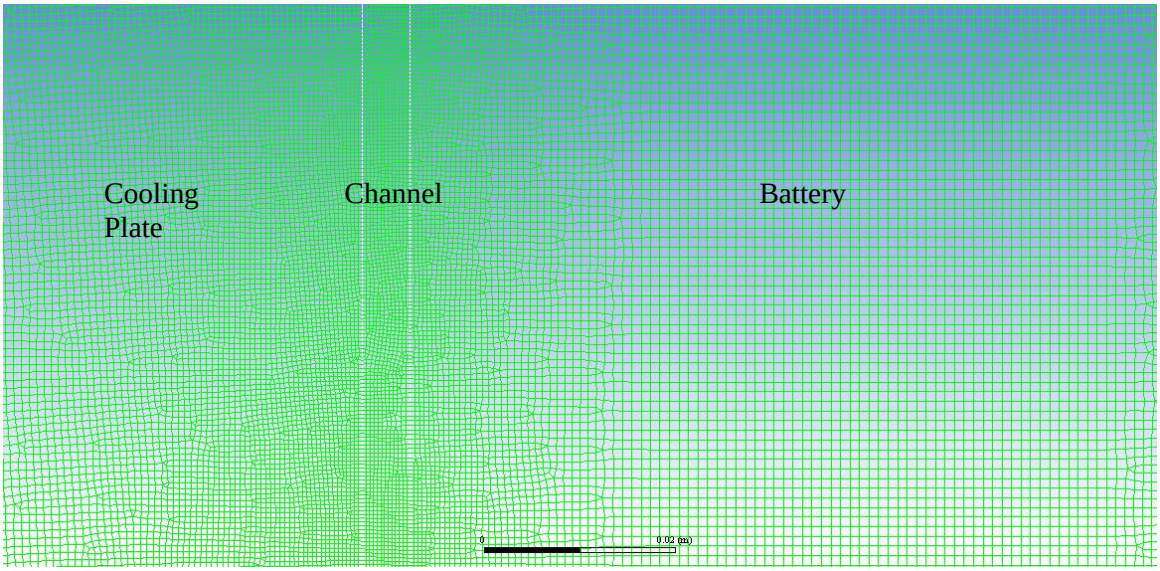

Figure 2-11: Detailed view of the mesh inside the system

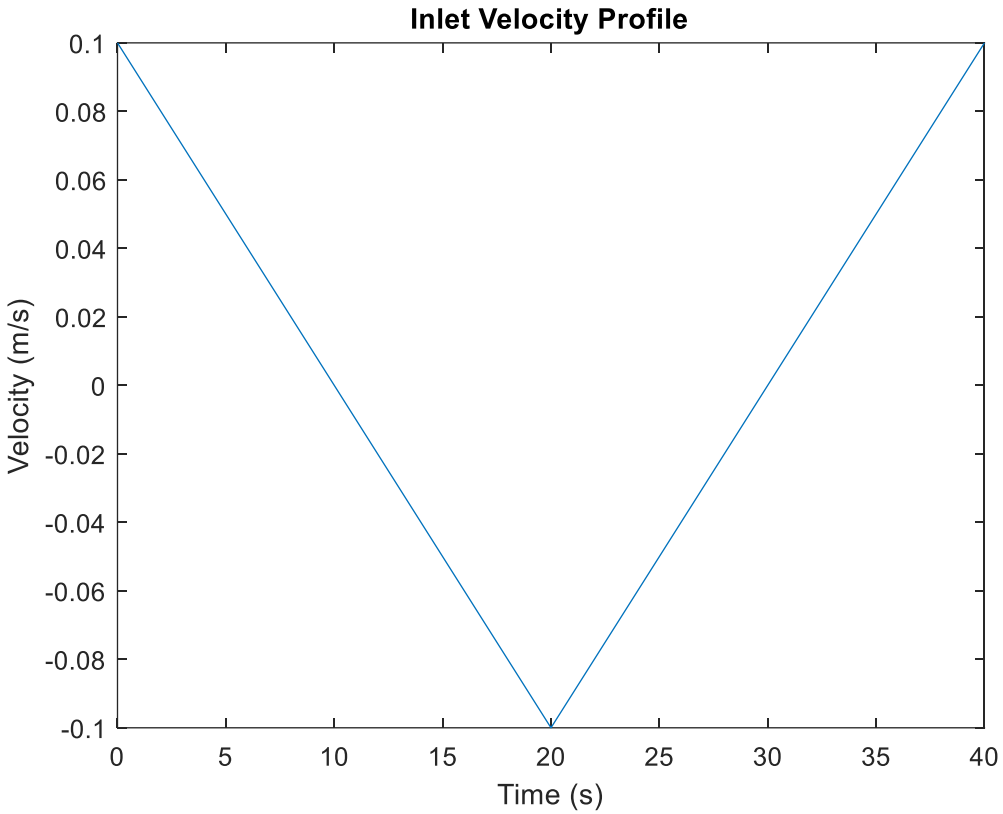

Figure 2-12: Inlet Velocity profile of the oscillatory flow (frequency = 0.025 Hz)

In this Chapter, the methods to be used in conducting the simulations were described, along with the problem setup. In the next Chapter, the results of these simulations are discussed.

Chapter 3: Result and Discussion

3.1 Validation of the 2D Fluidic Oscillator Model

This chapter begins with discussion of the results from the fluidic oscillator simulations. The model setup and operating conditions have been outlined in the previous chapter. Figure 3-1 shows the u-velocity (x-component of velocity) contour of the fluidic oscillator with inlet speed of 15.1716 m/s (Re = 30515). As demonstrated by the velocity contours, there is an oscillating sweeping jet that emerges out of the fluidic oscillator into the extended domain. There is also reverse circulation occurring in the feedback channel as fluid goes in the negative direction. This agrees with the previous descriptions in section 1.2. The reverse circulations deflects the stream near the power nozzle and results in an oscillatory sweeping jet. The sweeping jet's u-velocity is monitored at two virtual points, as shown in Figure 3-1. Figures 3-2 and 3-3 show a plot of the u-velocity at those two points versus time, when the inlet speed is at 15.1716 m/s (Re = 30515).

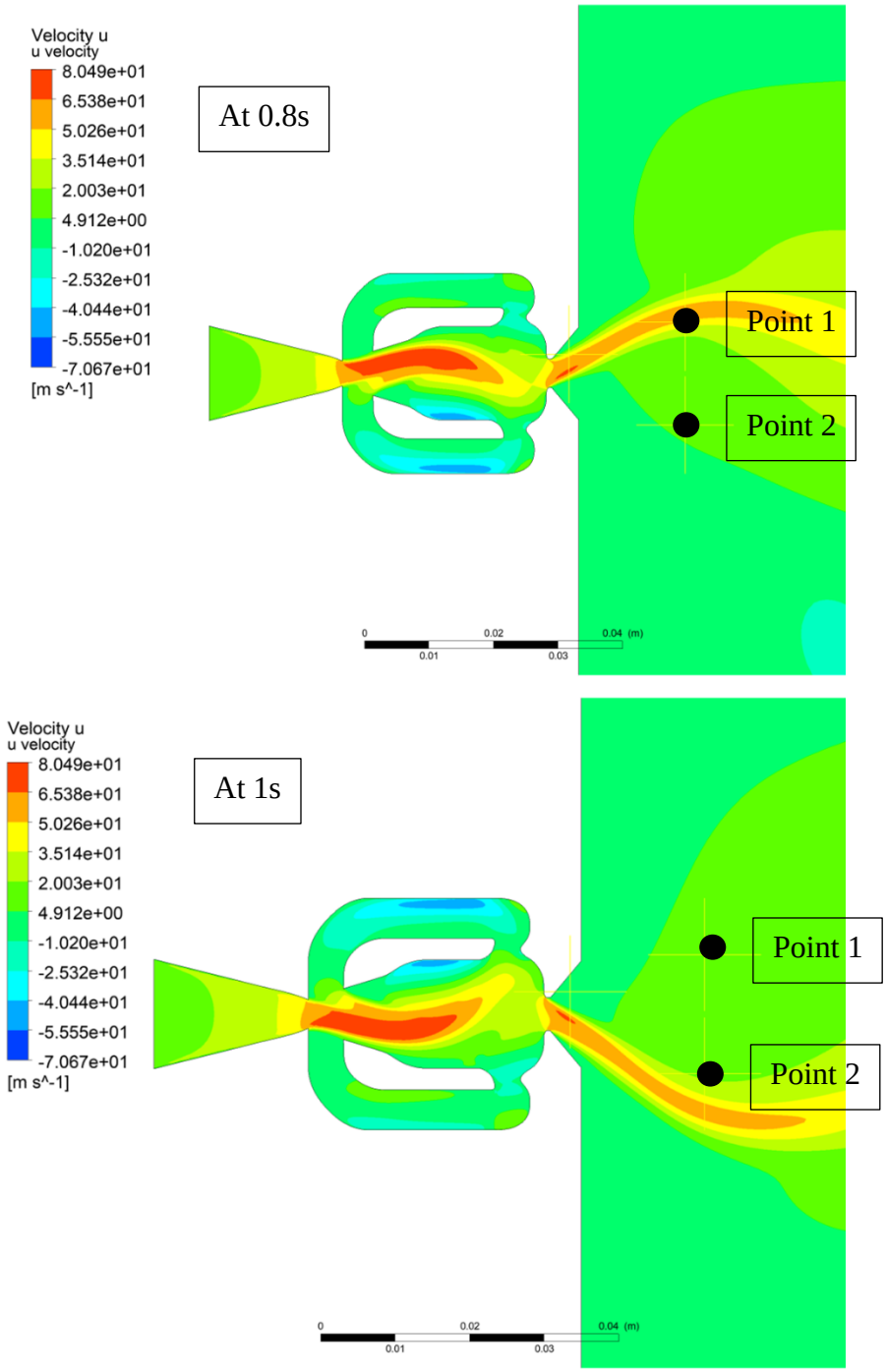

Figure 3-1: u-velocity contour of fluidic oscillator mode at different time (inlet Re = 30515)

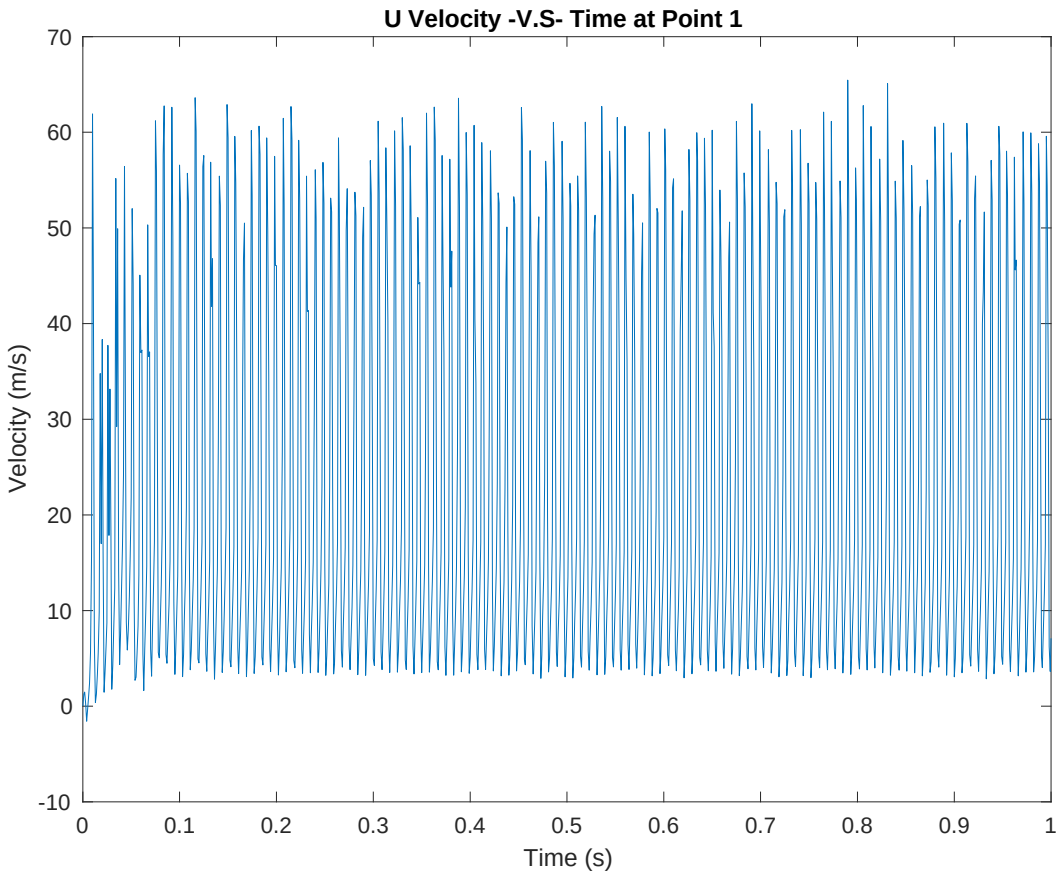

Figure 3-2: u-velocity versus time at point 1 (inlet speed = 15.1716 m/s)

These plots show that the u-velocity appears to behave in a periodic manner at both points, indicating that the exiting jet is oscillating. Observing the results from simulations with lower inlet speed (see Appendix section 4), the frequency of the periodic wave decreases, which is in agreement with the experimental data shown in Table 2-1. From the time-domain data shown in these two figures, it is difficult to determine the fundamental frequency of oscillation. Applying a Fast Fourier Transform, the amplitude spectra of those velocity data are computed and are shown in Figure 3-4.

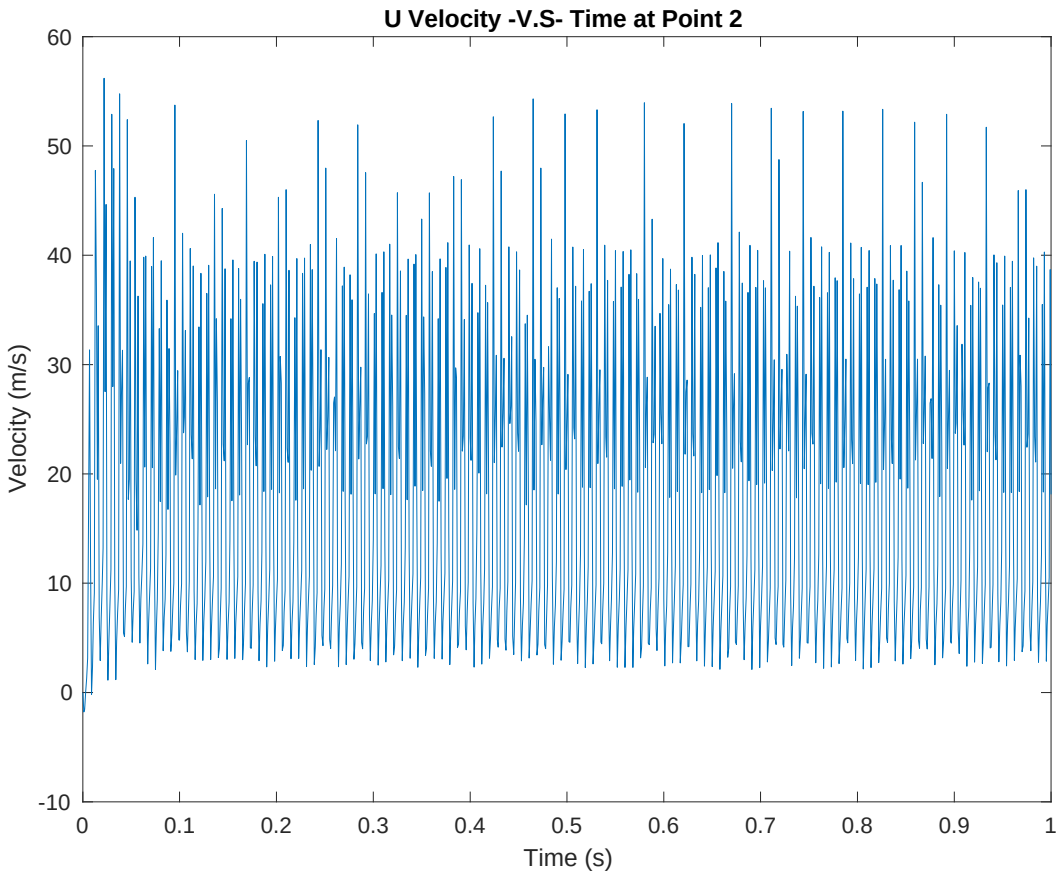

Figure 3-3: u-velocity versus time at point 2 (inlet speed = 15.1716 m/s)

From these two amplitude spectra (see Appendix section 5 for amplitude spectra from rest of simulations), the frequency at which the first amplitude peak occurs is very close for both points. The secondary peaks may be due to higher harmonics caused by local secondary recirculation. Therefore, in the current case, only the frequency of the first amplitude peak is relevant since the first amplitude peak is due to the main sweeping jet. The results are tabulated (see Appendix section 6).

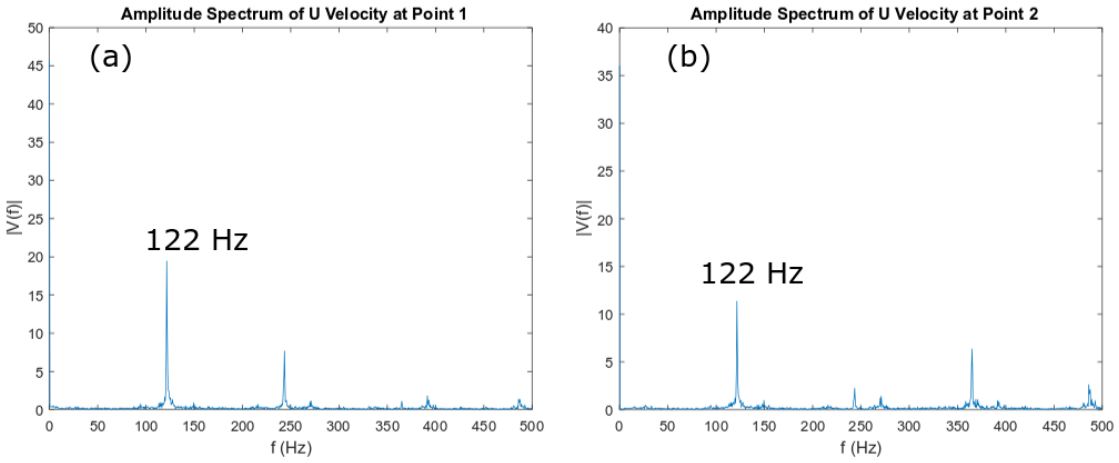

Figure 3-4: Amplitude spectrum of u velocity at (a) point 1 (b) point 2 (inlet speed = 15.1716 m/s)

From the table (see Appendix section 6 and Figure 3-6), there is a large difference between the computed and the experimentally recorded oscillation frequency. This may be attributed to two reasons: (1) the simulations were conducted in 2D, which is expected to significantly alter the system's response since viscous effects from the walls in the z-direction (depth) are absent, and (2) the method used to record the frequency in the experiments is different. In Hossain's experimental setup, the tool for measuring the oscillating frequency is a microphone (1/4" DeltaTron type 4954B) [7], which captures acoustic pressure waves from the sweeping jet. Nonetheless, the trend of the computed results agrees with the experimental observations. As the inlet speed increases, the oscillation frequency increases.

Figure 3-5 shows the plot of the oscillation frequency versus Reynolds number. The qualitative behavior is similar to that shown in Hossain's work (Figure 3-6). Initially, the Reynolds number and oscillation frequency have a linear increasing relationship (up to about Re = 16000), and then slowly becomes non-linear. Beyond about 16 m/s (Re ≈ 32000), an additional slope change is observed. In summary, although the computed oscillation frequencies are

somewhat different quantitatively from the experimentally observed frequencies, the qualitative behavior is the same, lending credibility to the computed results.

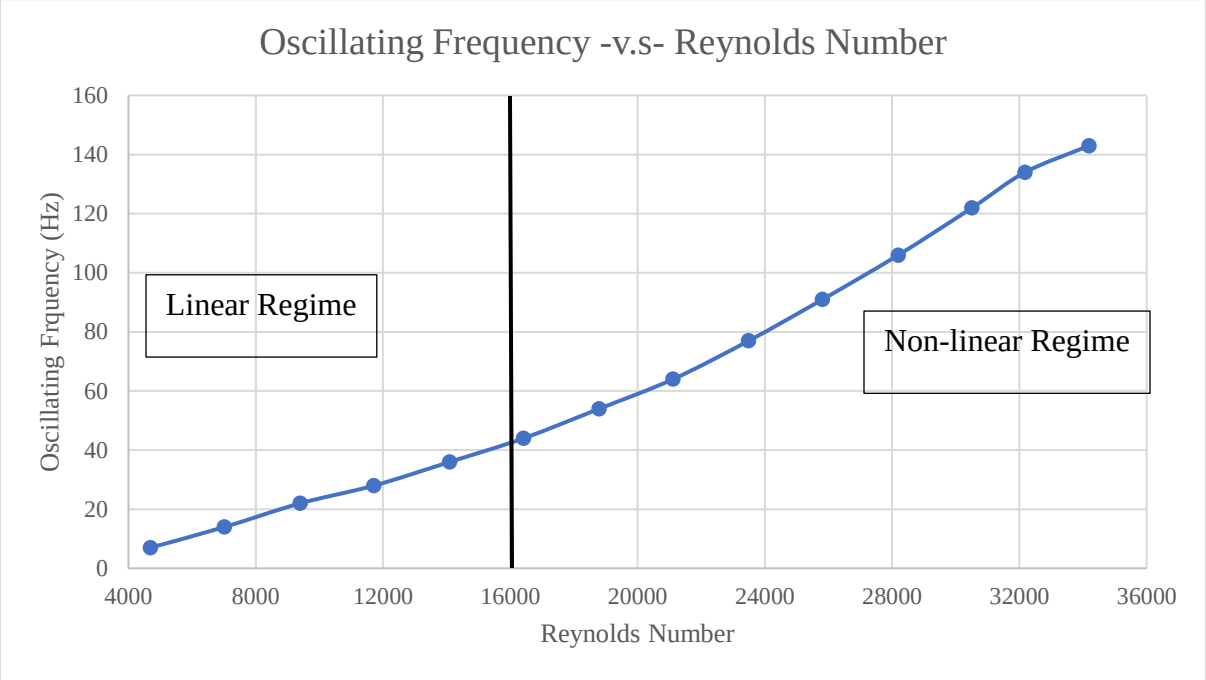

Figure 3-5: Oscillating Frequency versus Reynolds Number

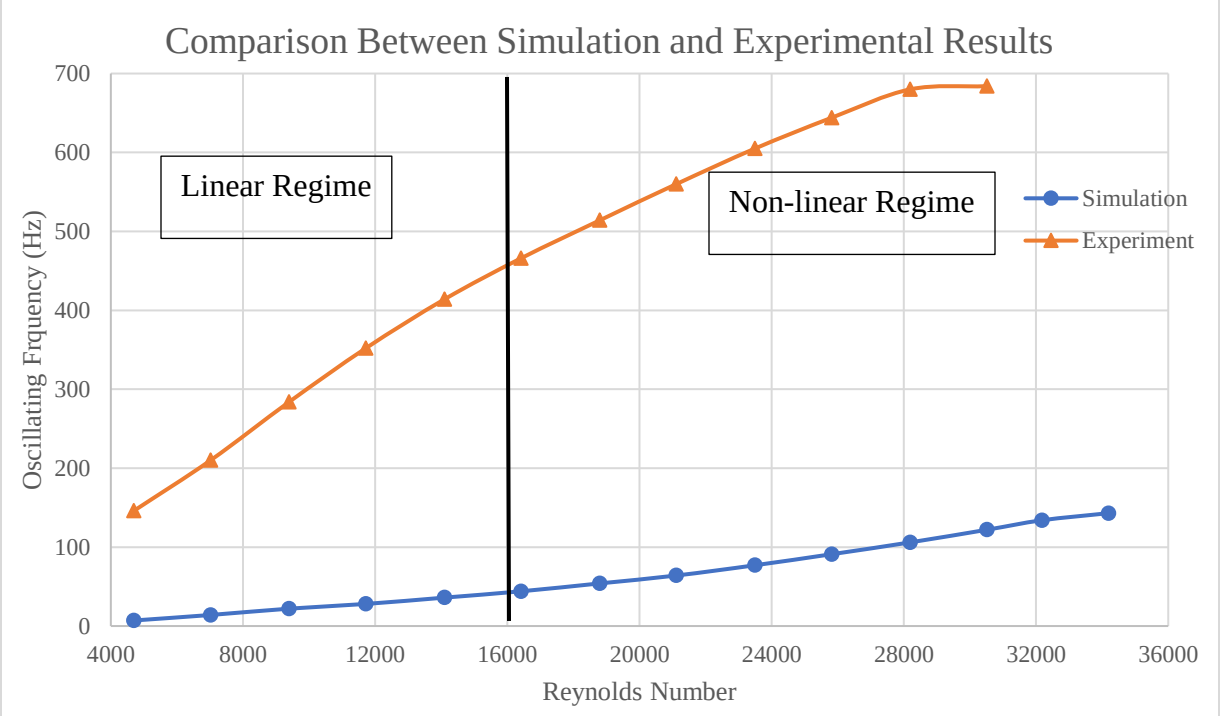

Figure 3-6: Comparison Between Simulation and Experimental Results [7]

3.2 Preliminary Study of Oscillatory Flow for Cooling

3.2.1 Variation of Channel Geometry

In this section, the investigations on cooling efficacy that were conducted with various channel configurations are reported. The inlet speed is set as 0.005 m/s (Re = 500), and the oscillatory flow changes the direction every 100s as the water reaches the opposite end of the channel. Volumetric heat source of the system is set as constant 1 kW/m^3. For all cases studied, the area-weighted average temperature of the cooling plate was recorded and plotted versus time.

For the U-shape channel configuration shown in Figure 2-7, cooling with oscillatory flow produced the lowest area-weighted average temperature, as shown in Figure 3-7. On the other hand, straight channels with either steady (unidirectional) or oscillatory flow exhibit similar cooling effect, as shown in Figure 3-7. This finding is in line with the hypothesis that secondary vortices enhance the heat transfer, and is likely to increase the cooling effect. Secondary vortices cannot form in straight channel, but are prevalent in bent channels around the bends. When flow reverses direction, these vortex structures are further stretched and results in enhanced mixing. Comparison of the top corner regions of the flow channels in Figure 3-8 shows that in the case of oscillatory flow, the corners have colder temperatures (blue color as compared to yellow), which implies a larger local temperature gradient between the hot plate and the cooling channel, and consequently, more effective heat removal.

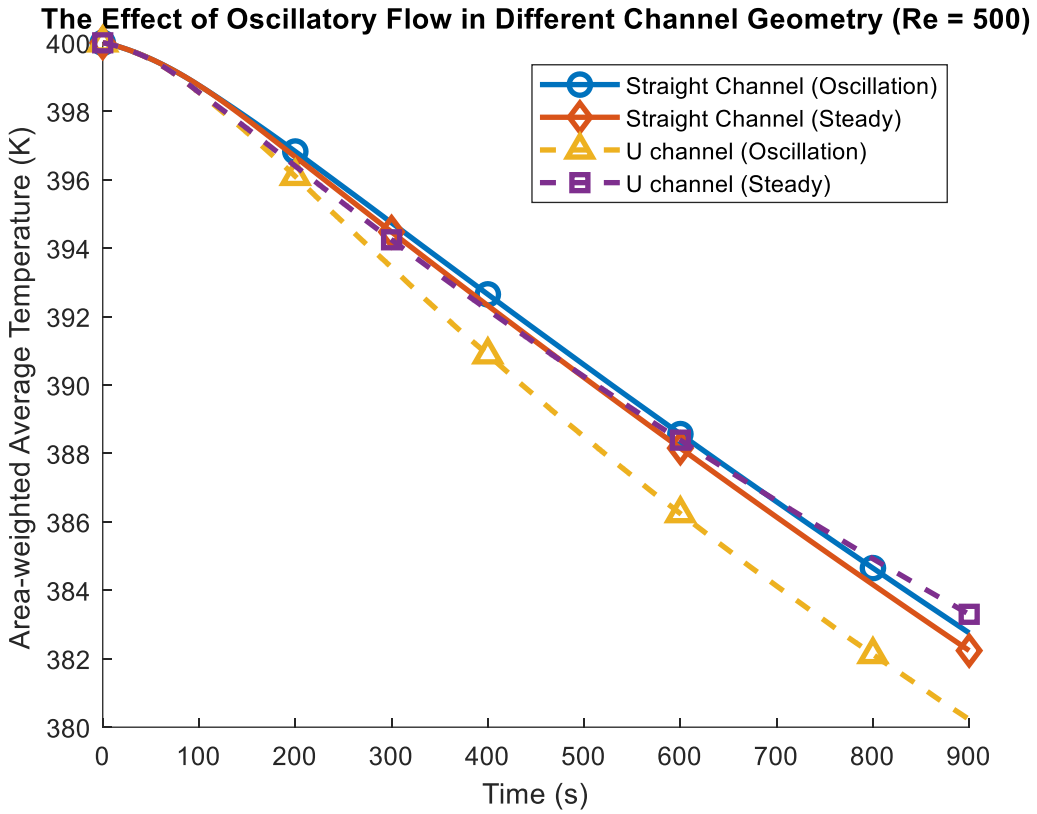

Figure 3-7: Cooling effect of oscillatory flow in different channel geometry (Re = 500)

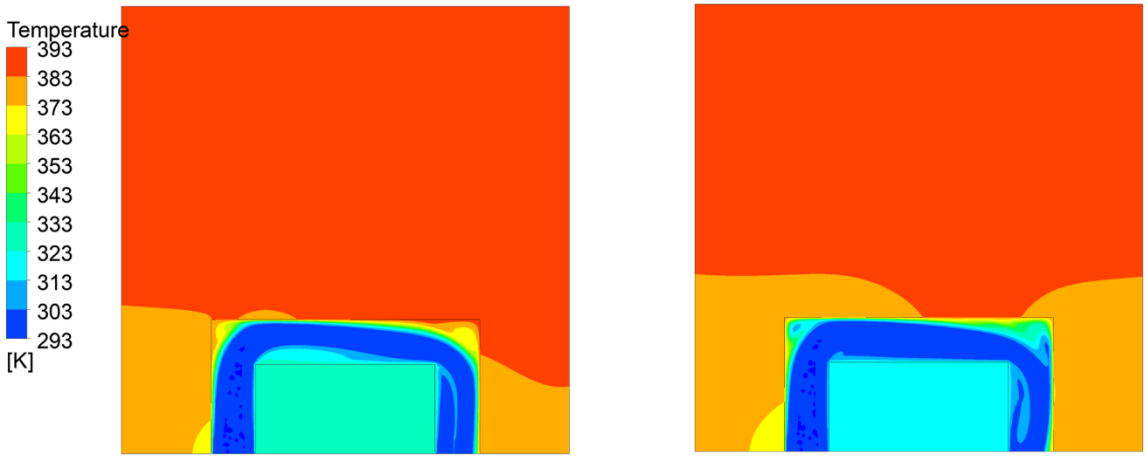

Figure 3-8: Temperature contour of the U-shaped channel system at 900s (left: unidirectional flow, right: oscillatory flow)

3.2.2 Effect of Turbulence

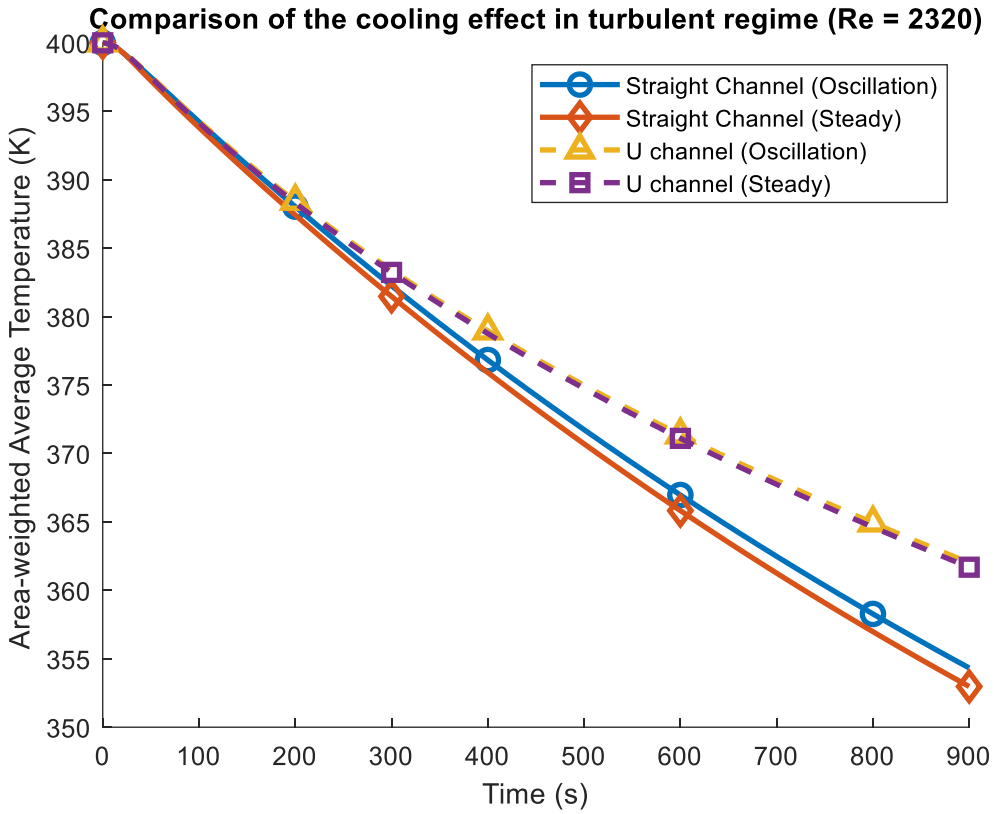

Figure 3-9: Comparison of the cooling effect in turbulent regime (Re = 2320)

In the preceding section, the channel configurations were compared for laminar flow. Next, the study is extended to turbulent flow. Figure 3-9 shows the results for the turbulent regime. Different than the previous results, the straight channel provides slightly better cooling than the U-shaped channel. The cooling effect difference between those two channel geometries is about 8 K. Along with that, the difference between steady and oscillatory flow in either system is found to be not as significant in turbulent regime. Perhaps, this is because the mixing due to the large-scale unsteadiness that was significant in the case of laminar flow, is exceeded by the mixing due to small-scale structures in the turbulent flow, as shown in Figure 3-10. Therefore, one cannot conclude that oscillatory flow is always advantageous for cooling. It appears to depend on the flow regime. Further investigations of additional channel designs are warranted to provide better understanding.

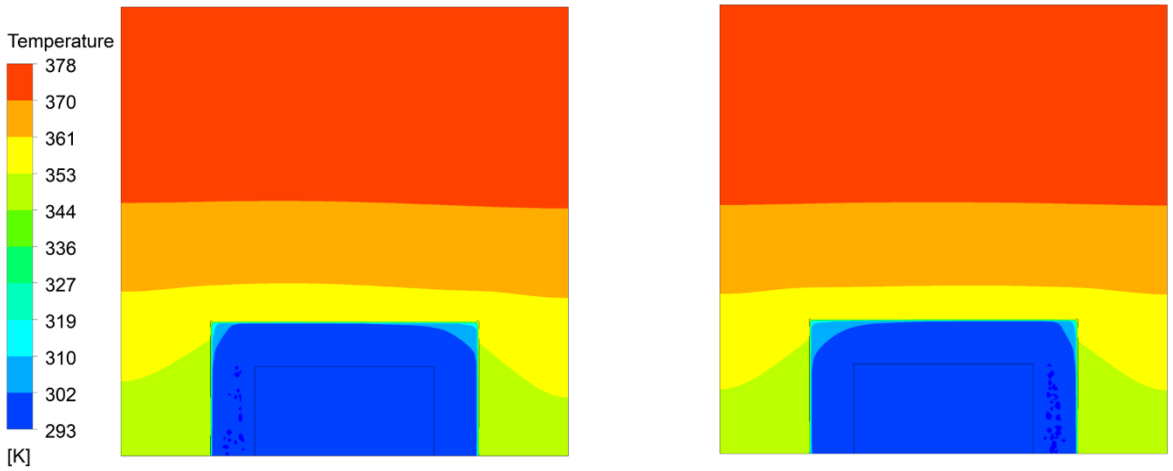

Figure 3-10: Temperature contour of the U-shaped channel system at 900s in turbulent regime (left: unidirectional flow, right: oscillatory flow)

3.2.3 Additional Channel Design

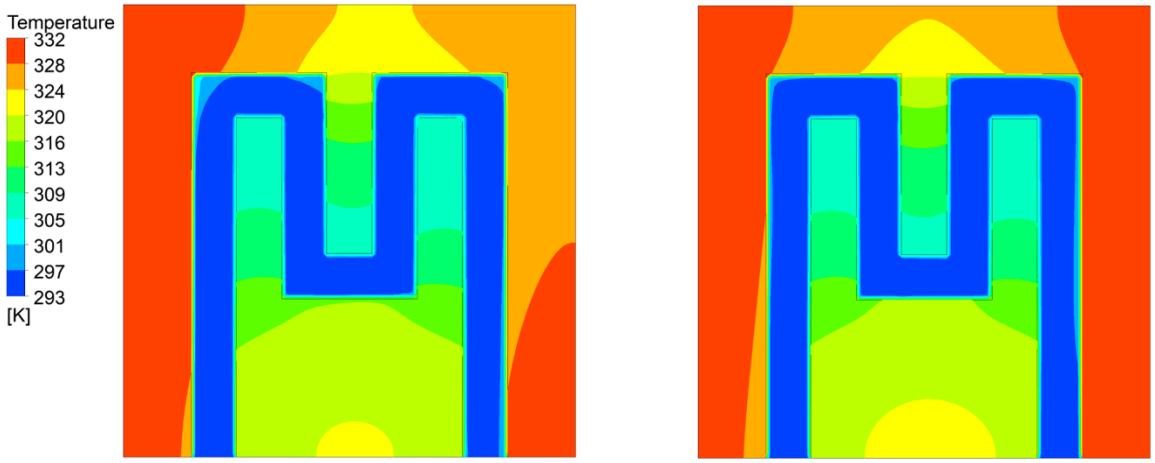

Figure 3-11: Temperature contour of the additional cooling system at 900s (left: unidirectional flow, right: oscillatory flow, frequency = 1/256 Hz)

Next, a design with a double-U bend was considered. Figure 3-11 shows a sample temperature contour from the simulations of the double-U bend channel. The figure shows that there is extended region into the plate that is cooled, which is different than the previous U-shape system. Different oscillation frequencies were tested, and Figure 3-12 shows the plot of area-weighted average temperature of the plate versus time. From the plot, one can observe that as the

oscillation frequency is decreased, the cooling effect improves but only up to a certain point. With frequency of $\frac{1}{256}\ Hz$, the oscillatory flow provides slightly better (about 1K) cooling effect than the unidirectional flow. This is due to switching the flow direction in high frequency may prevent the coolant from reaching the entire length of the channel before the flow switches direction; so some area of the plate is not cooled effectively. With a lower frequency, the flow reaches every part of the channel, which provides better cooling effect. However, there is a limit to which the frequency can be decreased. As the frequency reaches $\frac{1}{512}\ Hz$, the temperature change became less than 0.2 K. So, in this case, there is no significant advantage when an oscillating frequency lower than $\frac{1}{256}\ Hz$ is used.

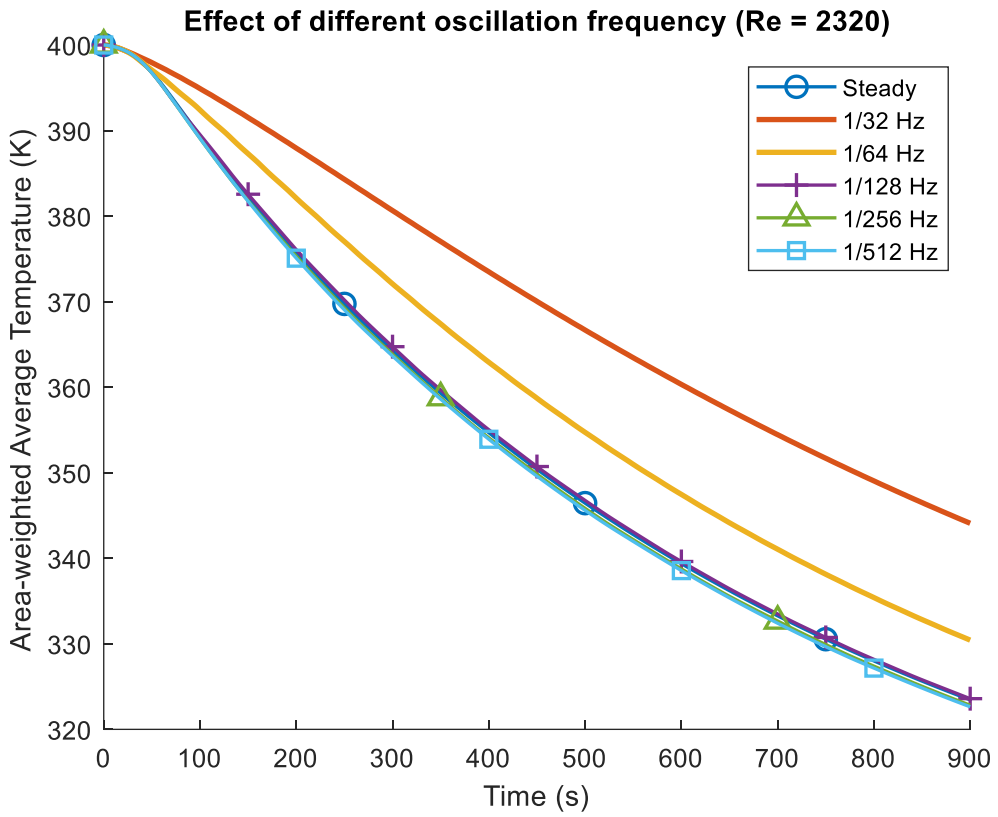

Figure 3-12: Effect of different oscillation frequency (Re =2320)

3.2.4 Investigation of Oscillatory Flow in an Application

In this section, we report the results obtained for the application described in Section 2.3.8. Specifically, we compare the differences between unidirectional flow and oscillatory flow. Figure 3-13 shows the results for this particular application (see Figure 2-10). Figure 3-13 shows that the oscillatory flow provides better cooling effect than the unidirectional flow, and the temperature difference at the end between steady flow and oscillatory flow is about 4 K. While using oscillatory flow, the area-weighted average temperature behaves in an oscillatory manner. This is because the magnitude of the inlet velocity is constantly changing, and so, the cooling capacity varies temporally. The effect of different oscillation frequency is not obvious in this case. Difference of area-weighted average temperature at 900s is within 1K between the different oscillation frequencies considered in this study.

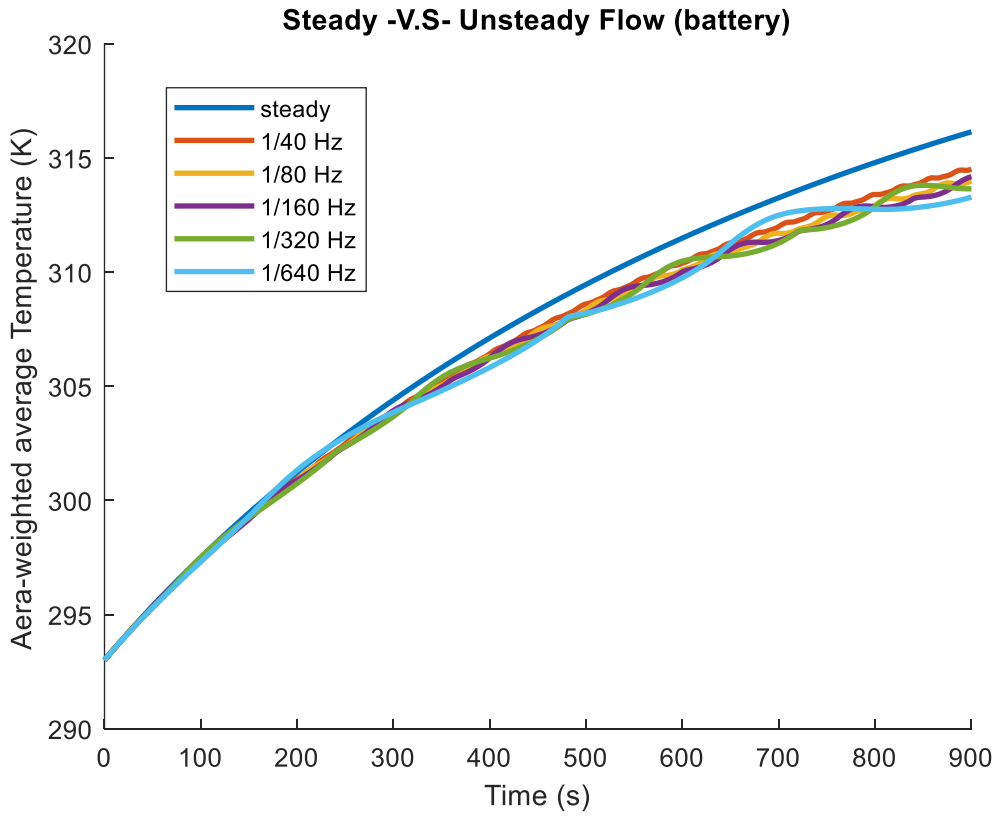

Figure 3-13: Comparison of oscillation frequency in the applicable cooling system

In the previous chapter, it was hypothesized that the use of oscillatory flow may prevent localization or stagnation of the hot spot, since the flow direction is switching constantly. In this particular application, it is anticipated that the battery packs on the two sides would cool almost evenly since there is no directional bias. To verify this hypothesis, a User-Defined function was written (See Appendix Section 3) to loop through all the cells (control volumes) in the battery, in order to find the cell with maximum temperature and its coordinate location. Figure 3-14 illustrates the max temperature locations detected within the entire battery between 500s – 900s.

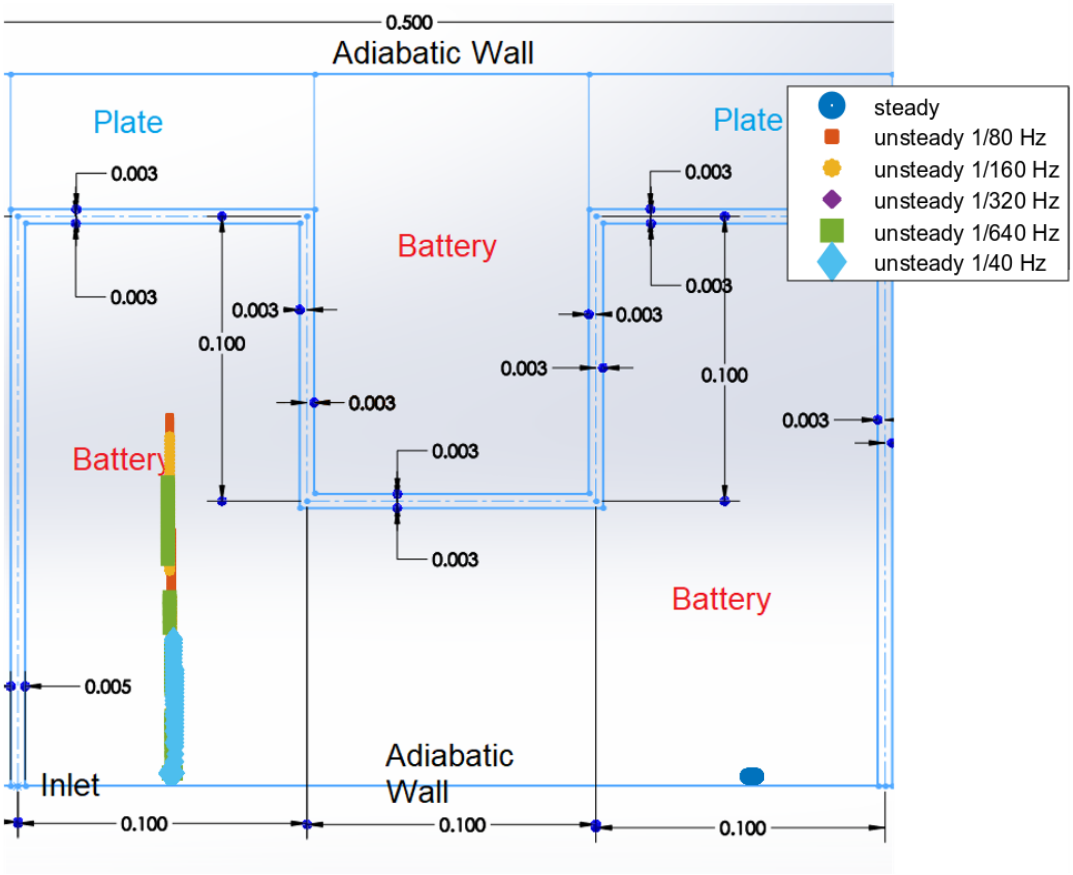

Figure 3-14: Max temperature location of the applicable cooling system after 500s

From Figure 3-14, it is clear that when cooling with unidirectional flow, the battery's maximum temperature location stays at the bottom of the right-side battery. This result is expected because as the coolant heats up, the cooling capacity near the outlet section (right side)

is not significant. Therefore, the bottom section of the battery (downstream end of cooling channel) has the highest temperature since the cooling capacity is the lowest. This can be also observed in the temperature distribution of the entire system, shown in Figure 3-15.

When oscillatory flow is used, the maximum temperature location switches position, which is expected due to constant changing of flow direction and the incoming cold fluid directly affecting the cooling capacity. Figure 3-14 shows that the maximum temperature location is always on the left battery. This may be counter-intuitive. In reality, the highest temperature in the left battery and right battery are within 10^{-3}K. However, since the user-defined function always picks the highest temperature, it displays the spot corresponding to the highest temperature only, giving the impression that the hot spot is always on the left battery. In reality it is on both batteries, and moves in the y-direction as shown in Figure 3-14. Figure 3-15, which depicts the temperature distribution, shows that cooling with oscillatory flow also creates a more even temperature distribution in the entire battery pack. With unidirectional flow, the left battery always has lower temperature than the right battery and the hot spot always resides on the right battery. The stagnation of the hot spot may lead to the failure of the system.

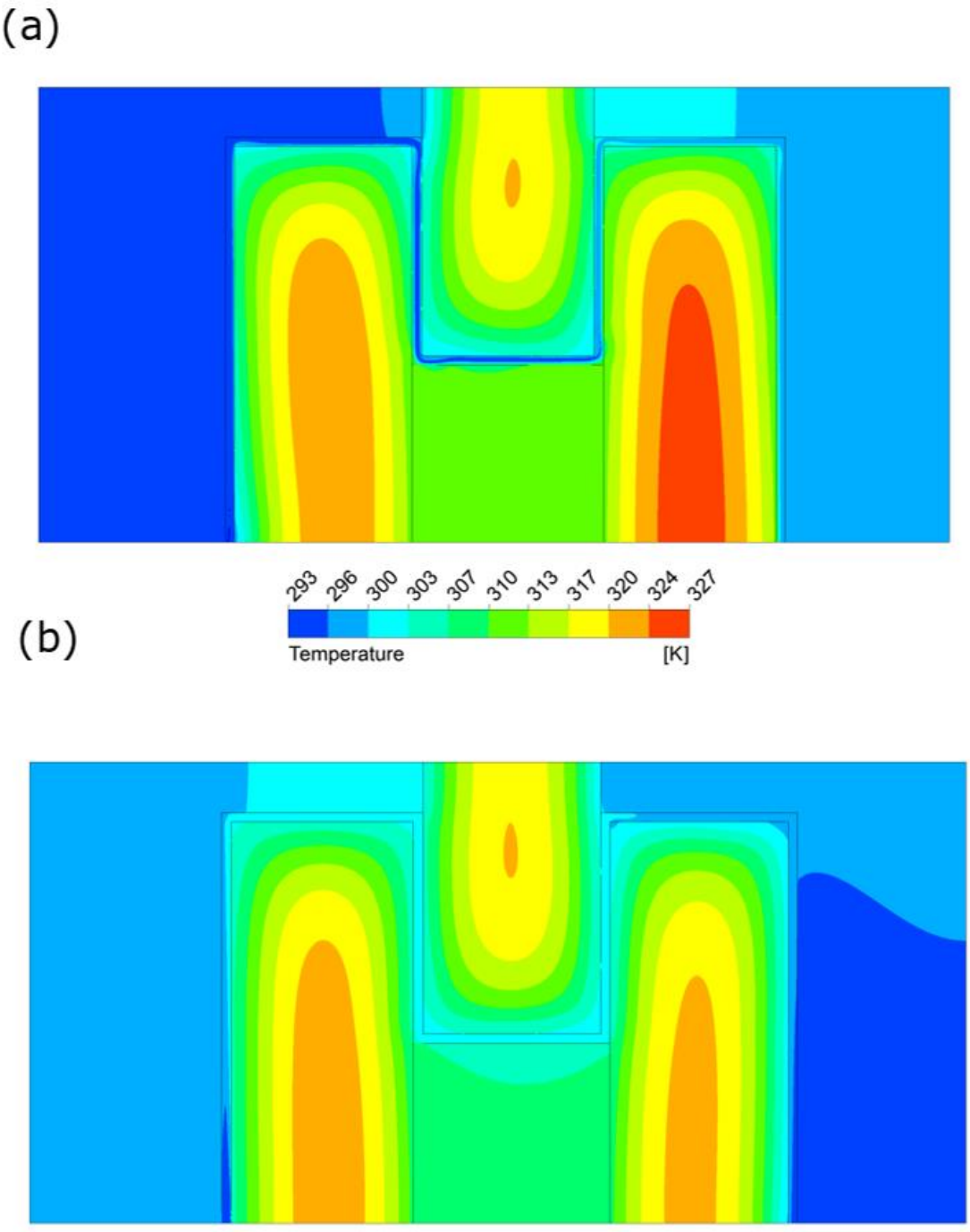

Figure 3-15: Temperature contour of the applicable cooling system at 900s (a. steady flow, b. oscillatory flow, 0.0125 Hz)

Chapter 4: Summary and Conclusions

In this thesis, a new cooling technique based on oscillatory flow was investigated. The study began with CFD simulations to understand the operating behavior of a fluidic oscillator, which is a device that can be used to reverse flow direction without additional power and moving parts. A 2D CFD model was developed based on the experimental studies of a fluidic oscillator conducted by Hossain [7], and validated against the same experimental data [7] by running series of simulations with the same inlet conditions as in Hossain's experiments [7].

It was found that the two-dimensional CFD model of the fluidic oscillator results in some differences between the simulation results and the experimental results—in particular, the predicted oscillation frequency versus flow rate (or Reynolds number). This is likely due to the fact that in the 2D model viscous effects from the walls in the z-direction (depth) are missing, and affects the performance of fluidic oscillator. Nonetheless, the qualitative trend of the predicted results agreed with the experimental observations. As the inlet velocity increases, the oscillating frequency of the sweeping jet increases linearly and then exhibits a nonlinear trend. Therefore, the 2D model can still be considered a valid model for preliminary study of the fluidic oscillator. In the future, generating a 3D model would be desirable, and a similar simulation strategy can be applied to validate the model.

Next, CFD/CHT analyses were conducted to explore the effect of oscillatory flow on cooling. This part of the study began with evaluating the effect of oscillatory flow in different channel configurations on cooling. A system with a straight coolant channel and a system with an U-shape coolant channel were first investigated. Simulations of both systems were conducted with unidirectional (steady) and oscillatory flow in the laminar regime. The area-weighted average temperature of the target (system being cooled) was computed and recorded.

Unidirectional and oscillatory flows in the turbulent regime were also investigated in the same system, and the same quantity was compared.

Following these preliminary investigations, an additional design with a double-U bend was also investigated. In this system, oscillatory flow with different oscillation frequencies was tested and the corresponding area-weighted average temperatures at the end of simulations were recorded and compared to understand the effect of oscillation frequency on cooling. Finally, a specific cooling application was considered. The model system was that of a cooling system for an electric vehicle's battery pack. This cooling system was simulated with a unidirectional flow and different oscillation frequencies, as well. Area-weighted average temperature was again recorded, along with the maximum temperature's (or hot spot's) location within the system.

Preliminary studies with various cooling channel designs, specifically one used for cooling a battery pack in an automotive application, showed that oscillatory flow provides advantages in cooling over unidirectional flow. The advantages are lower average temperature of the target body, and more uniform temperature distribution throughout the system. The model further shows that the maximum temperature point (or hot spot) in a system constantly shifts when cooling with oscillatory flow. This may prevent failure of a component since a stagnated hot spot in a component often leads to failure. To optimize the cooling performance, the inlet speed should make the flow near the turbulent regime. One important finding of the study is that the flow direction should be reversed only after the injected flow reaches the other end of the channel.

Further studies are warranted to understand the behavior of the fluidic oscillator as well as the cooling system using 3D models, along with integration of the fluidic oscillator model to the cooling model. Due to the time constraints and resource limitations, the integration of the

system could not be studied in this project. The following system, shown in Figure 4-1, is proposed as a potential integrated design for future testing. In this design, the fluidic oscillator is connecting to a 0.25 m x 0.25 m aluminum cooling plate with a 5 mm coolant channel. The fluidic oscillator outputs a sweeping jet at a certain frequency to evenly cool down the plate, so that the upper part of the channel may encounter larger flow rate and lower part of the channel may encounter smaller flow rate, or vice versa. One critical aspect of this design that requires careful investigation of how the frequency of the jet's sweeping may be matched with the frequency required for effective cooling. Using a similar strategy as described in Chapter 2, the effect of turbulent flow and oscillation frequency can be tested, along with finding the most suitable parameters to provide the best cooling effect.

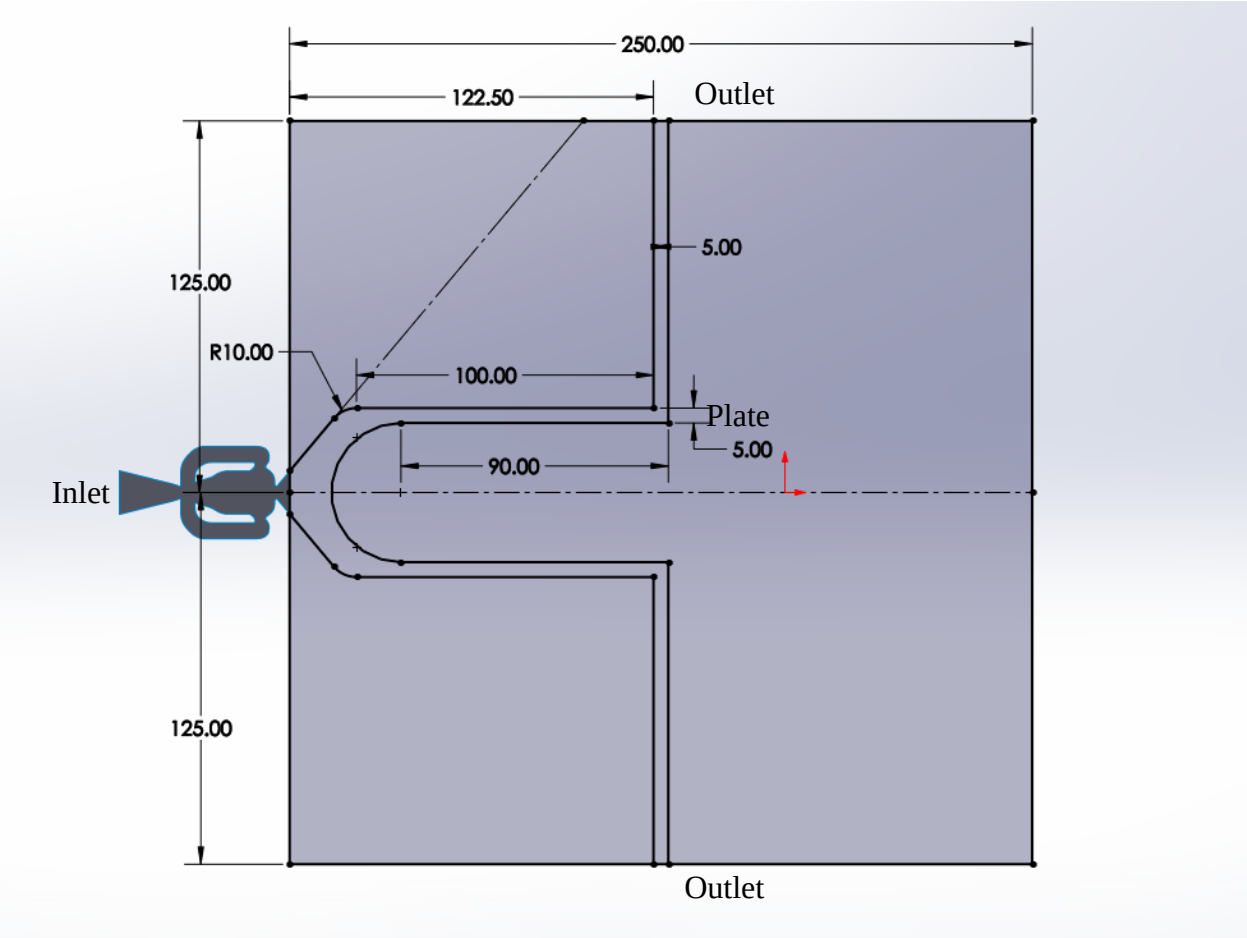

Figure 4-1: Completed cooling circuit (units in mm)

Reference

[1] P. Merkli, H. Thomann, Transition to turbulence in oscillating pipe flow, *Journal of Fluid Mechanics* **68**, 567-575 (1975).

[2] M. Ohmi, M. Iguchi, K. Kakehashi, T. Masuda, Transition to turbulence and velocity distribution in an oscillating pipe flow, *Bulletin of JSME* **25**, 365-371 (1982).

[3] M. Hino, M. Kashiwayanagi, A. Nakayama, T. Hara, Experiments on the turbulence statistics and the structure of a reciprocating oscillatory flow, *Journal of Fluid Mechanics* **131**, 363-400 (1983).

[4] R. Akhavan, R.D. Kamm, A.H. Shapiro, An investigation of transition to turbulence in bounded oscillatory Stokes flows part 1. experiments, *Journal of Fluid Mechanics* **225**, 395-422 (1991).

[5] F.A.Z.M. Saat, A.J. Jaworski, Numerical predictions of early stage turbulence in oscillatory flow across parallel-plate heat exchangers of a thermoacoustic system, *Applied Sciences* **7**, 673 (2017).

[6] M. Sieber, F. Ostermann, R. Woszidlo, K. Oberleithner, C.O. Paschereit, Lagrangian Coherent Structures in the Flowfield of a Fluidic Oscillator, Gallery of Fluid Motion, 68th Annual Meeting of the APS Division of Fluid Dynamics, (2015), DOI: https://doi.org/10.1103/APS.DFD.2015.GFM.V0015

[7] M. A. Hossain, R. Prenter, L. Agricola, R. Lundgren, A. Ameri, J. Gregory, J. Bons, Effects of Roughness on the Performance of Fluidic Oscillators, 55th AIAA Aerospace Sciences Meeting, (2017), DOI: https://doi.org/10.2514/6.2017-0770

[8] *ANSYS FLUENT 12.0 Theory Guide*, Release 12.0, ANSYS, Inc., Jan 23rd, 2009. Accessed on Mar 7th, 2020. [Online]. Available: https://www.afs.enea.it/project/neptunius/docs/fluent/html/th/main_pre.htm

[9] C. Arcus, "Tesla Model 3 & Chevy Bolt Battery Packs Examined," *CleanTechnica*, 27-Sep-2019. [Online]. Available: https://cleantechnica.com/2018/07/08/tesla-model-3-chevy-bolt-battery-packs-examined/. [Accessed: 16-Mar-2020].

[10] C. Lin, S. Xu, and J. Liu, "Measurement of heat generation in a 40 Ah LiFePO4 prismatic battery using accelerating rate calorimetry," *International Journal of Hydrogen Energy*, vol. 43, no. 17, pp. 8375–8384, 2018.

[11] B. Wu, Y. Ren, and N. Li, "LiFePO4 Cathode Material," *IntechOpen*, 06-Sep-2011. [Online]. Available: https://www.intechopen.com/books/electric-vehicles-the-benefits-and-barriers/lifepo4-cathode-material. [Accessed: 17-Mar-2020].

Appendix

1. Converting the 3D Mass Flow Rate to 2D Inlet Velocity

Assume mass conservation of the system,

$$\dot{m} = \rho_{air} u A$$

So, the Reynolds number equation becomes,

$$Re = \frac{\rho_{air} u D_{h,3D}}{\mu_{air}} = \frac{\frac{\dot{m}}{A} \cdot \frac{4A}{P}}{\mu_{air}} = \frac{4\dot{m}}{P \cdot \mu_{air}} = \frac{\rho_{air} u D_{h,2D}}{\mu_{air}}$$

$$u = \frac{4\dot{m}}{P \cdot \rho_{air} \cdot D_{h,2D}}$$

Where the 2D hydraulic diameter $D_{h,2D}$ calculated based on

$$D_{h,2D} = \frac{4A}{P} = \frac{4(H * W)}{2 * (H + W)} = \frac{4H}{2 * (\frac{H}{W} + 1)}$$

Since the model is 2D

$$\lim_{W \to \infty} \frac{4H}{2 * (\frac{H}{W} + 1)} = 2H$$

Therefore,

$$u = \frac{4\dot{m}}{P \cdot \rho_{air} \cdot 2H}$$

In those equations,

$\dot{m}$ = mass flow rate ($\frac{kg}{s}$),

u = velocity ($\frac{m}{s}$),

A = cross section area of the fluidic oscillator ($1.681 * 10^{-5}\ m^2$)

Re = Reynolds number,

ρ_{air} = the density of air ($1.225 \frac{kg}{m^3}$),

$D_{h_{3D}}$ = hydraulic diameter in 3D model (m),

$D_{h_{2D}}$ = hydraulic diameter in 2D model (m),

μ_{air} = dynamic viscosity of the air ($1.7894 * 10^{-5}\ \frac{kg}{m \cdot s}$),

P = wetted perimeter ($0.03758\ m$),

H = throat height of fluidic oscillator (m),

W = throat width of fluidic oscillator (m).

2. FLUENT Commands for Switching the Flow Directions

/define/boundary-conditions/zone-type 13 pressure-outlet

/define/boundary-conditions/pressure-outlet 13 y n 0 n 293 n y n n n y 5 0.1 y

/define/boundary-conditions/zone-type 14 velocity-inlet

/define/boundary-conditions/velocity-inlet 14 n n y y n 0.02331 n 0 n 293 n n n y 5 0.1

/define/boundary-conditions/zone-type 13 velocity-inlet

/define/boundary-conditions/velocity-inlet 13 n n y y n 0.02331 n 0 n 293 n n n y 5 0.1

/define/boundary-conditions/zone-type 14 pressure-outlet

/define/boundary-conditions/pressure-outlet 14 y n 0 n 293 n y n n n y 5 0.1 y

3. FLUENT User-Defined Function for Returning the Max Temperature Cell Location

```
# include "udf.h"
// Find the location of the max temperature cell in the battery
DEFINE_EXECUTE_AT_END(execute_at_end)
{
        FILE *fmax_location;
        Domain *domain = Get_Domain(1);
        Thread *t_battery = Lookup_Thread(domain,12);
        cell_t c;
        real xc[2];
        double max_temp, t, x, y;

        max_temp = 293;
        t = CURRENT_TIME;
```

```
        begin_c_loop(c,t_battery)
        {
                if(C_T(c,t_battery) > max_temp){
                        max_temp = C_T(c,t_battery);
                        C_CENTROID(xc,c,t_battery);
                        x = xc[0];
                        y = xc[1];
                }
        }
        end_c_loop(c,t_battery)

        Message("Location of the max temperature: %f        %f\n",x,y);

        /*Data Output*/
        fmax_location = fopen ("Max temperature location.txt","a");

        if(fmax_location == NULL)
        {
        Message("Error, no file has been found\n");
        }

        fprintf (fmax_location,"%f                %f                %f\n",t,x,y);

        fclose(fmax_location);
        //#endif
}
```

4. U Velocity Plot at Point 1&2 of Fluidic Oscillator Model With Different Inlet Speed

Inlet speed = 2.3364 m/s

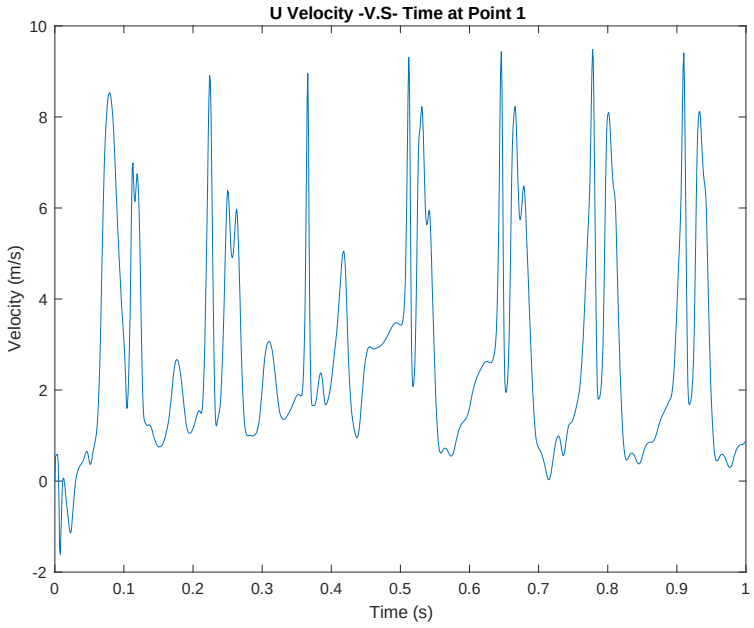

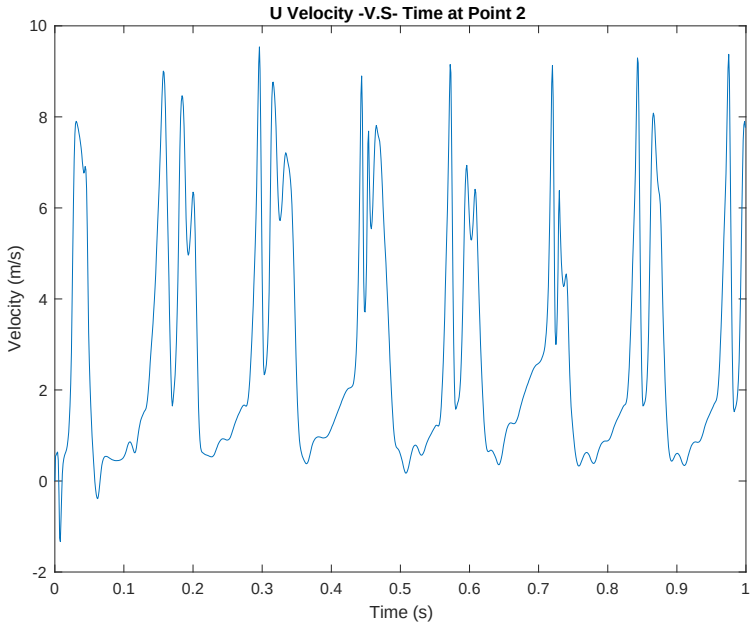

Inlet speed = 3.4898 m/s

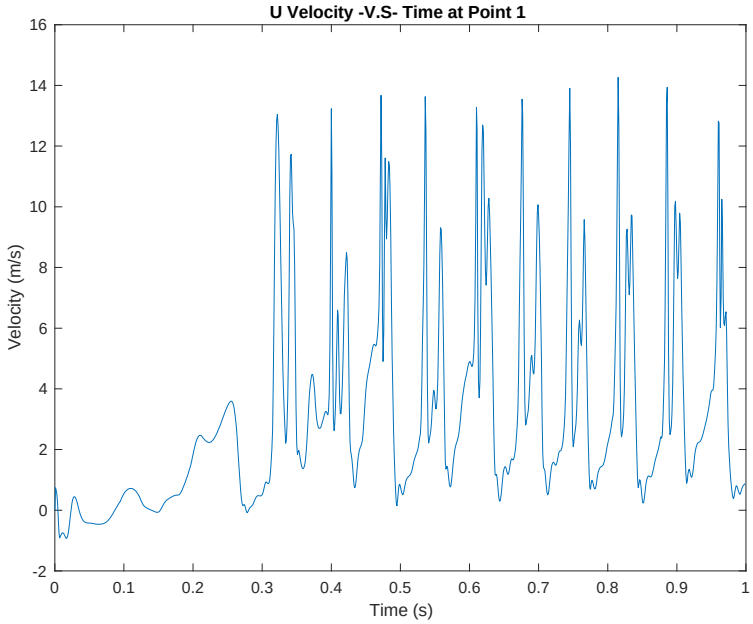

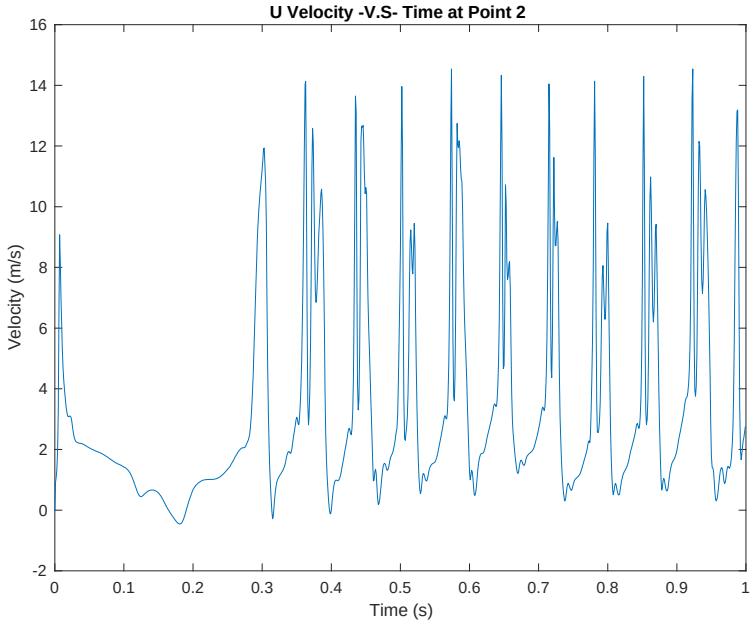

Inlet speed = 4.6727 m/s

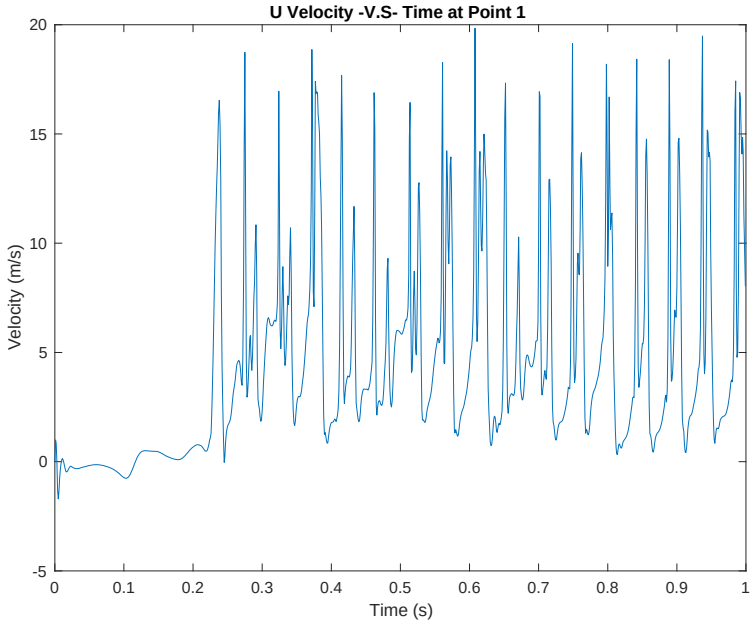

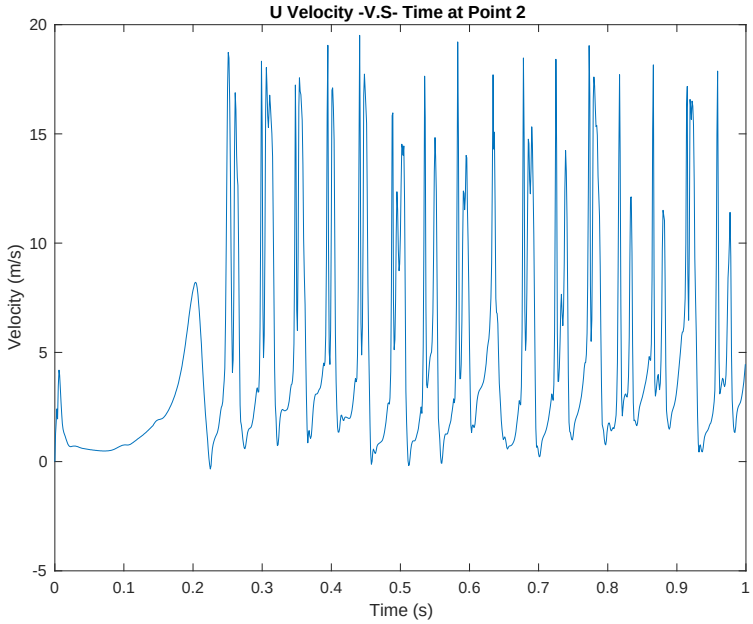

Inlet speed = 5.8261 m/s

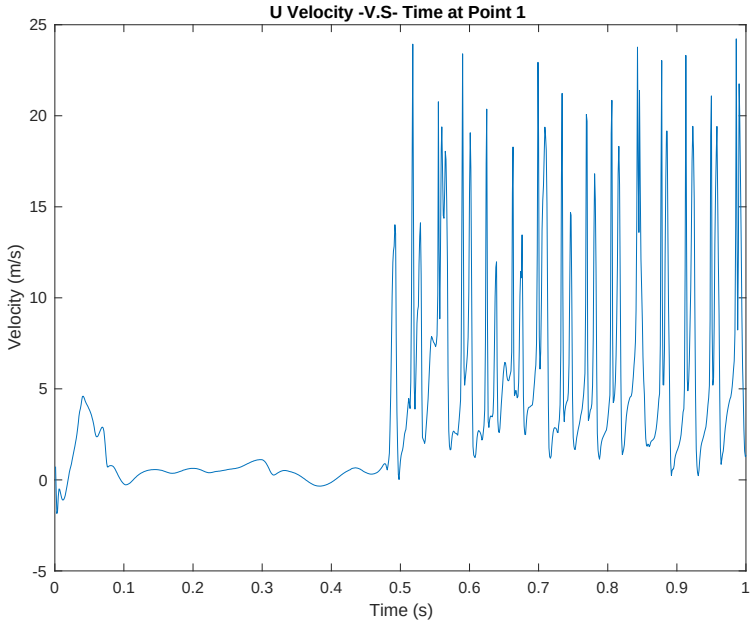

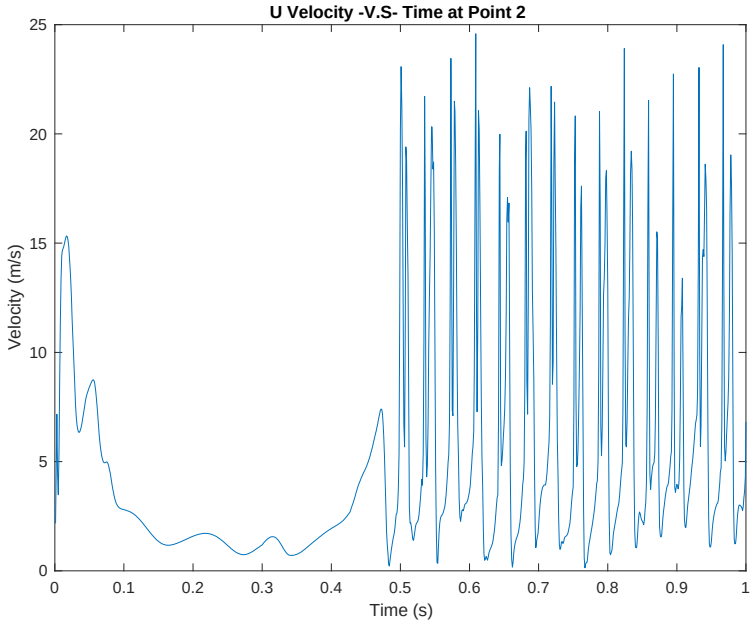

Inlet speed = 7.0091 m/s

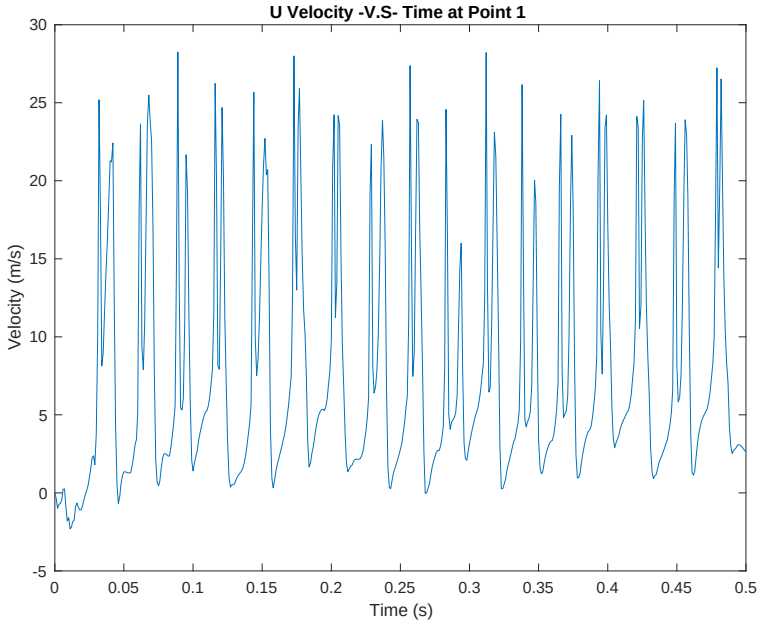

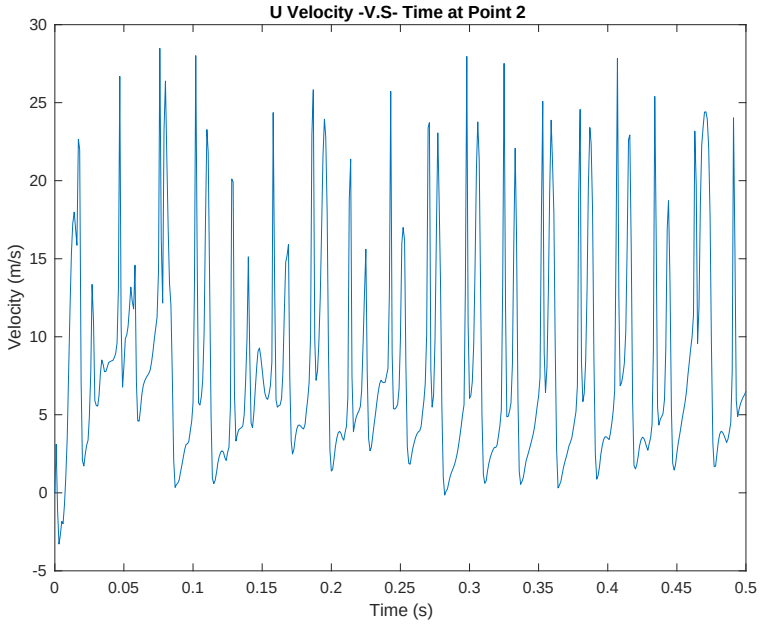

Inlet speed = 8.1625 m/s

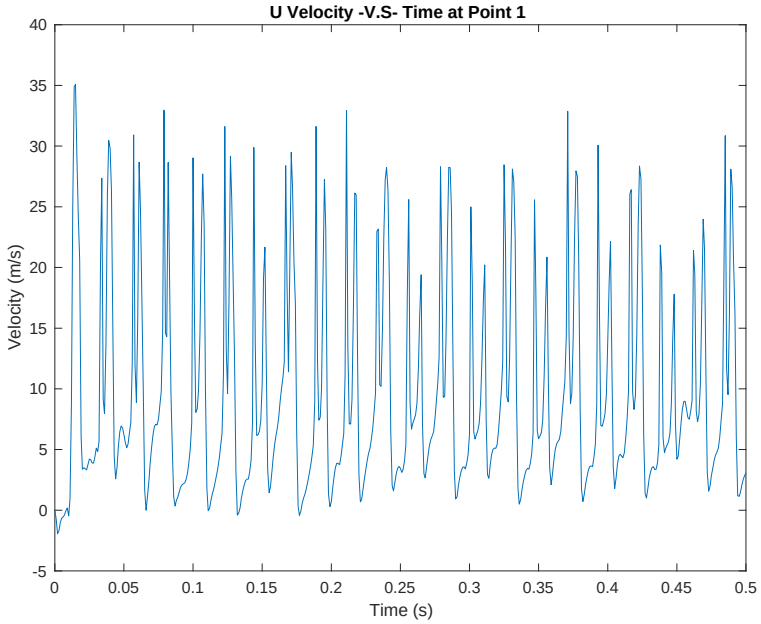

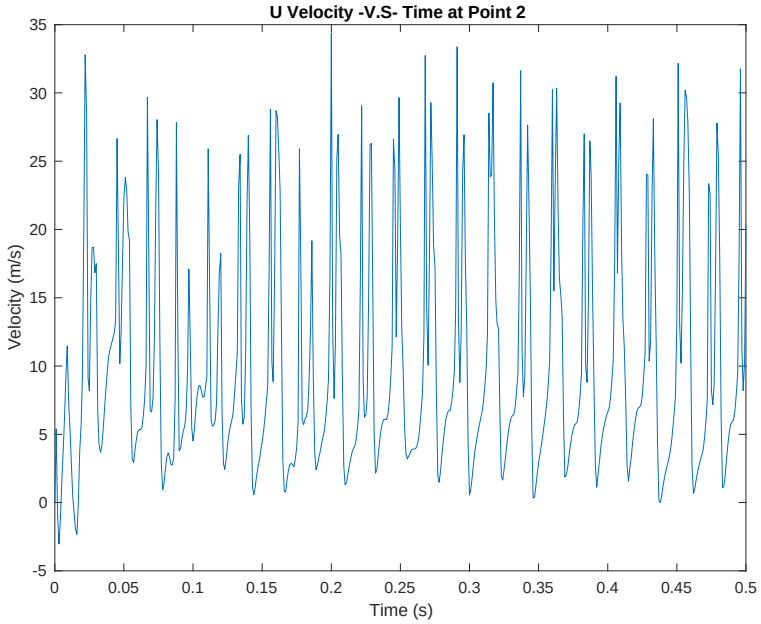

Inlet speed = 9.3455 m/s

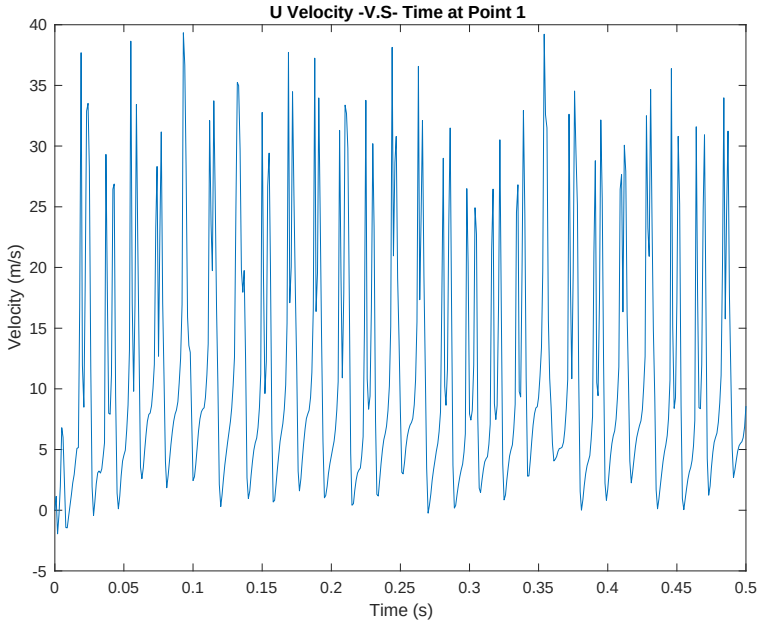

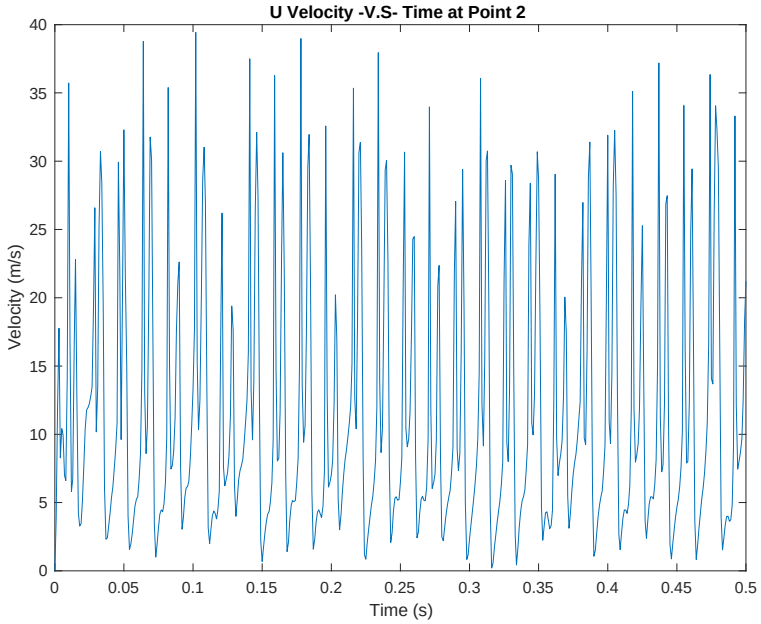

Inlet speed = 10.4989 m/s

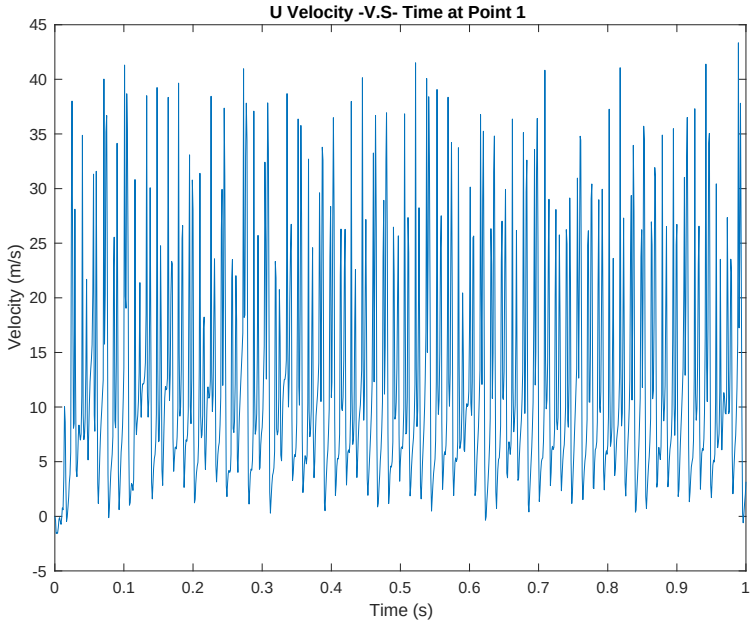

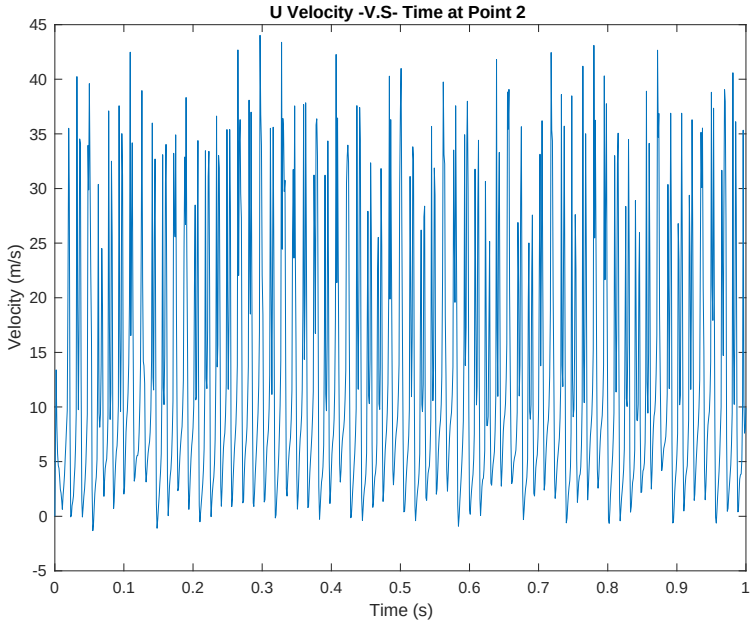

Inlet speed = 11.6819 m/s

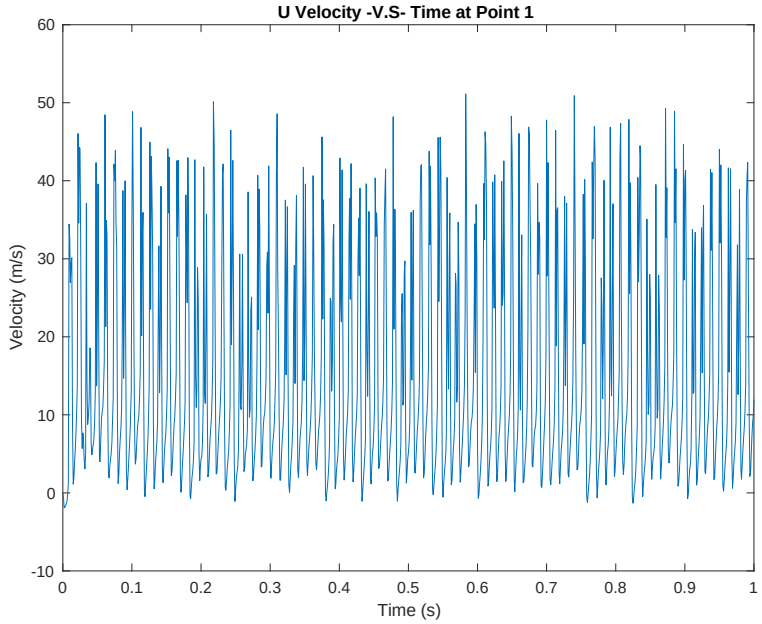

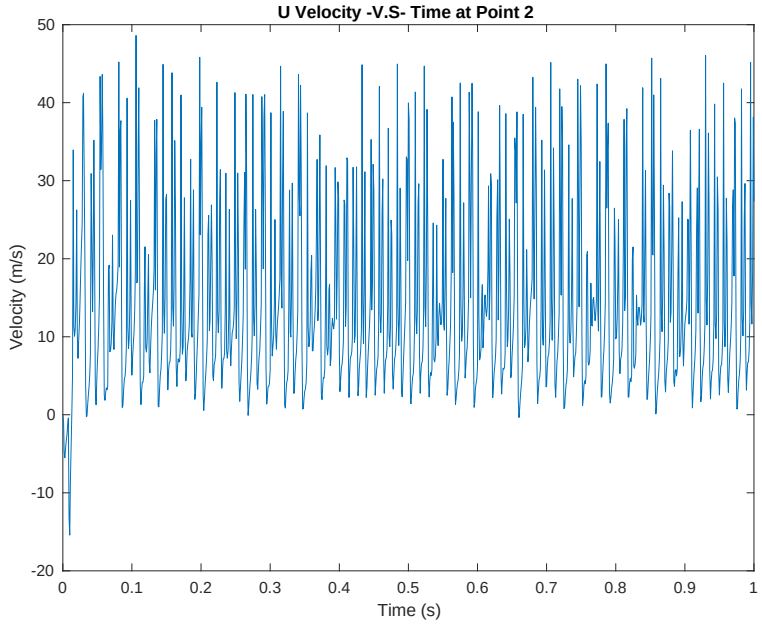

Inlet speed = 12.8353 m/s

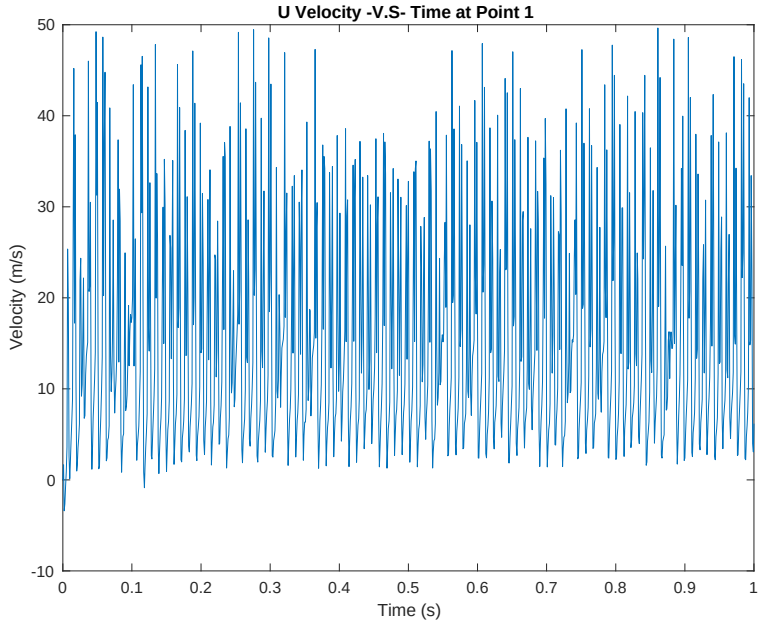

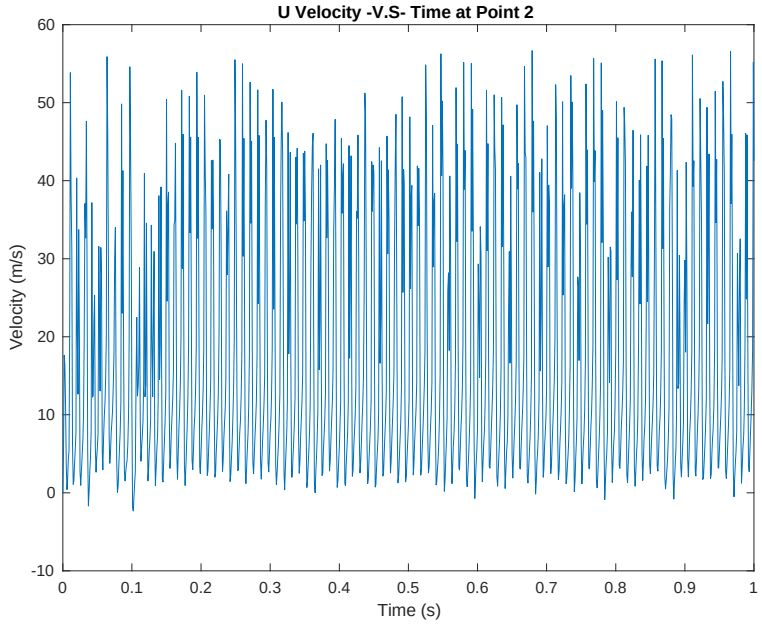

Inlet speed = 14.0182 m/s

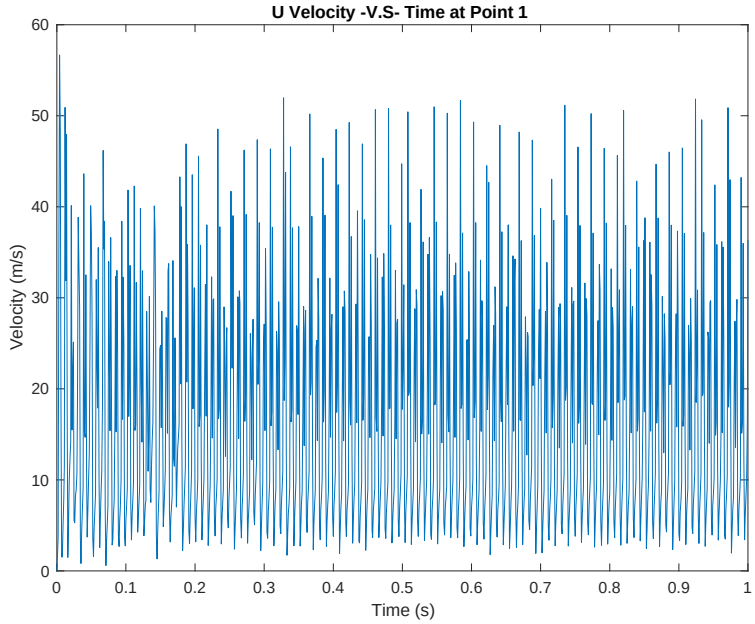
U Velocity -V.S- Time at Point 1
Velocity (m/s)
Time (s)
0
10
20
30
40
50
60
0
0.1
0.2
0.3
0.4
0.5
0.6
0.7
0.8
0.9
1

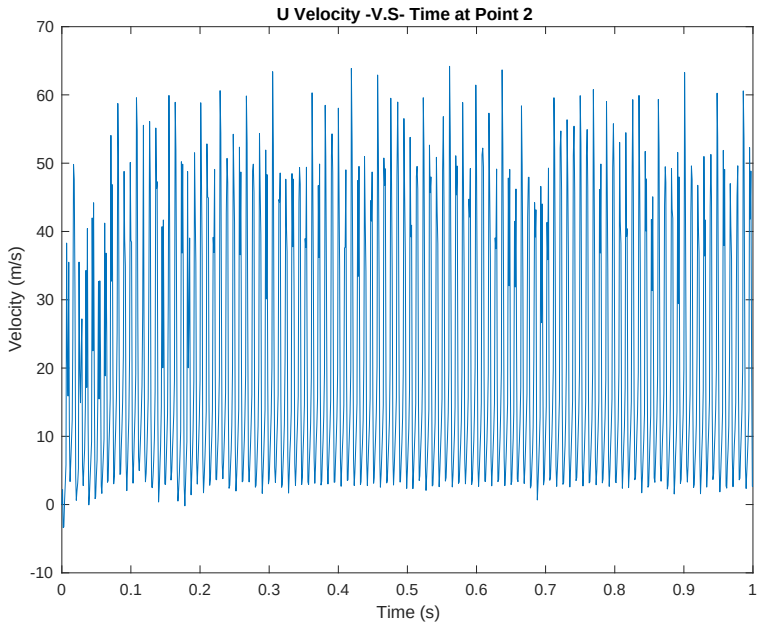
U Velocity -V.S- Time at Point 2
Velocity (m/s)
Time (s)
-10
0
10
20
30
40
50
60
70
0
0.1
0.2
0.3
0.4
0.5
0.6
0.7
0.8
0.9
1

5. Amplitude Spectrum at Point 1&2 of Fluidic Oscillator Model with Different Inlet Speed

Inlet speed = 2.3364 m/s

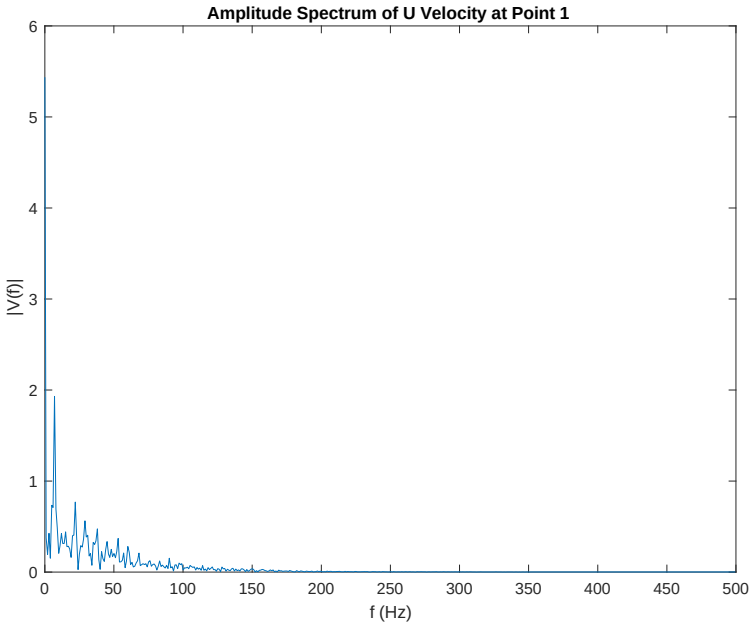

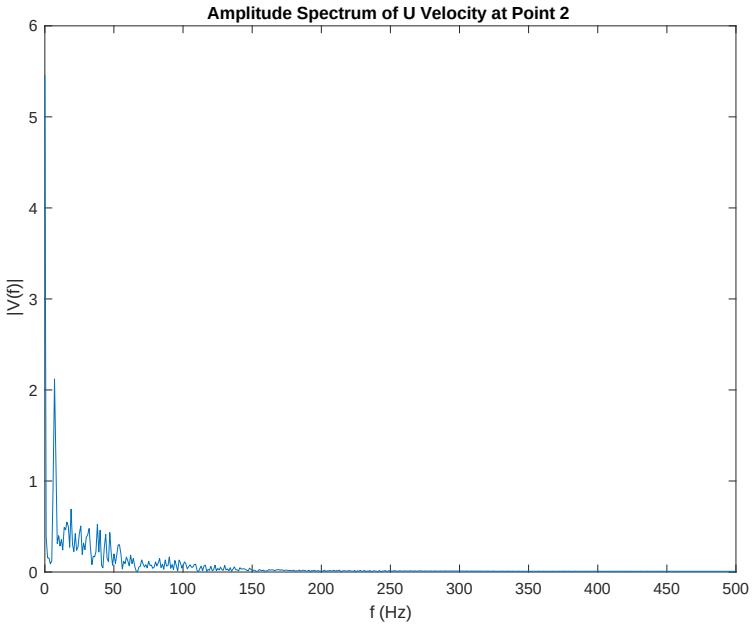

Inlet speed = 3.4898 m/s

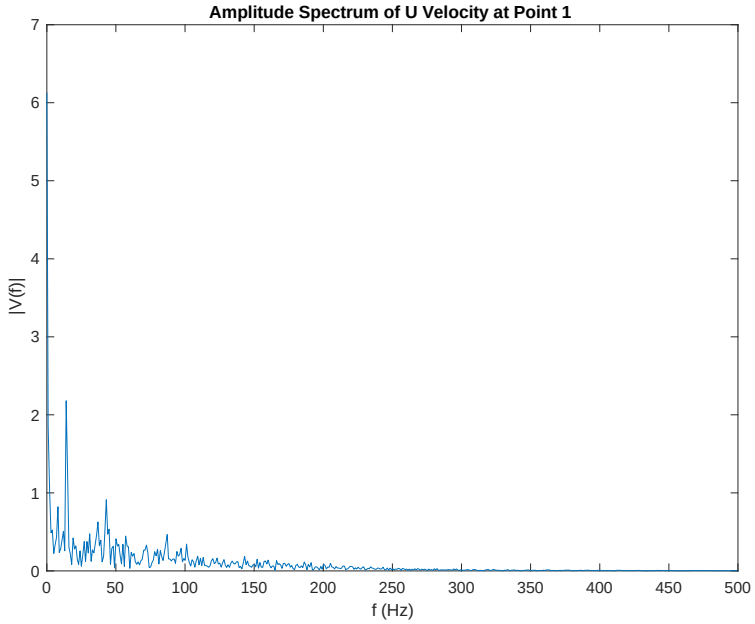

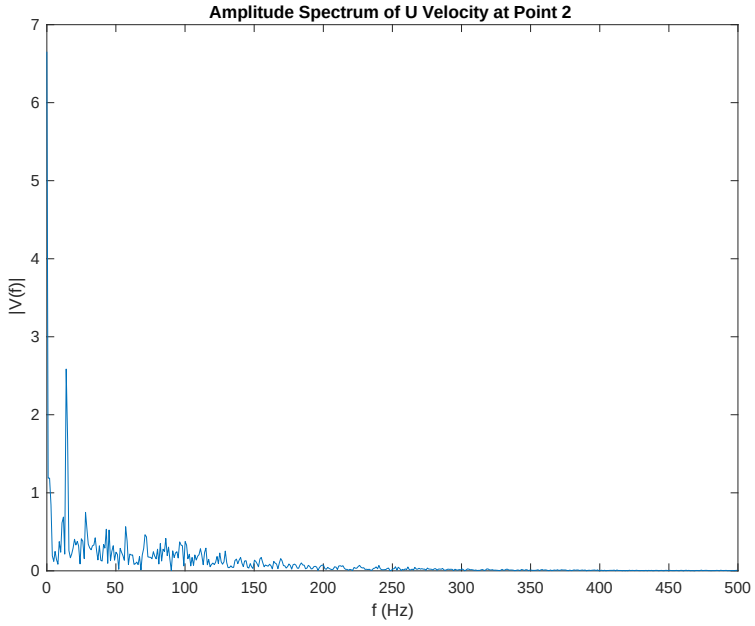

Inlet speed = 4.6727 m/s

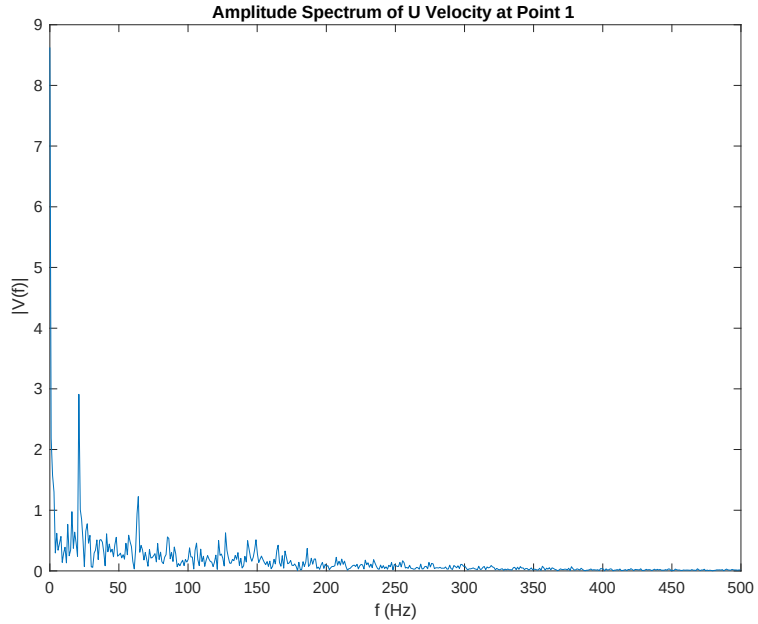

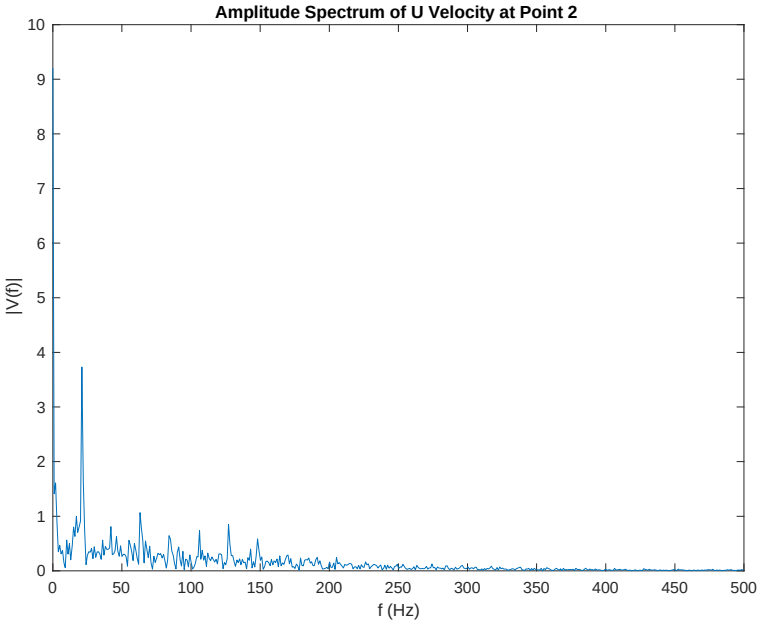

Inlet speed = 5.8261 m/s

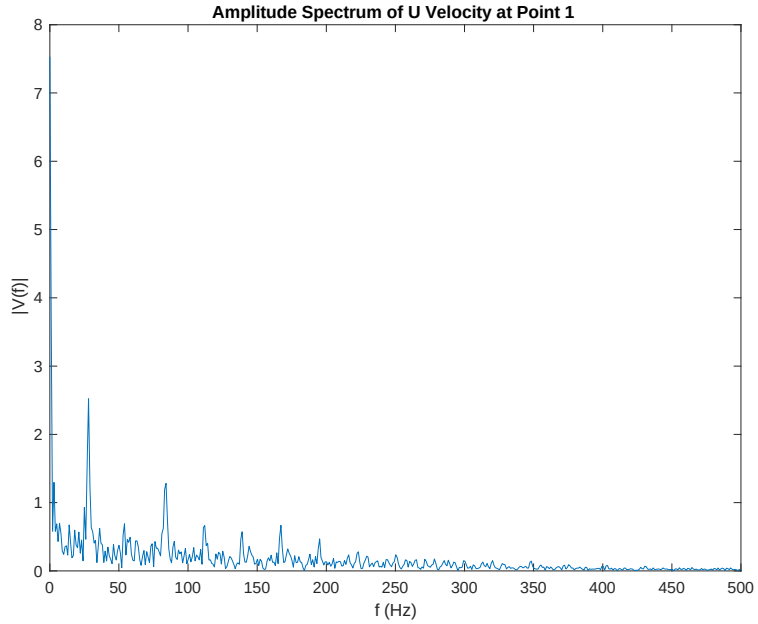

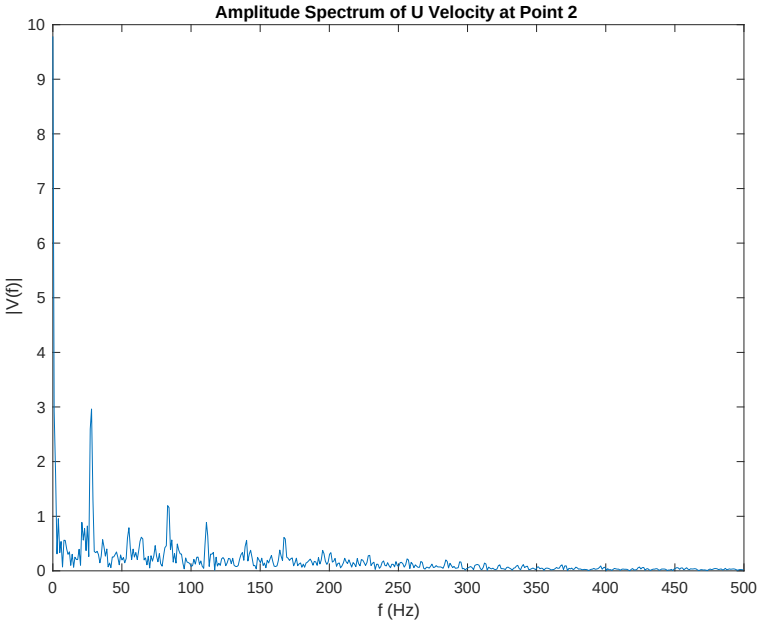

Inlet speed = 7.0091 m/s

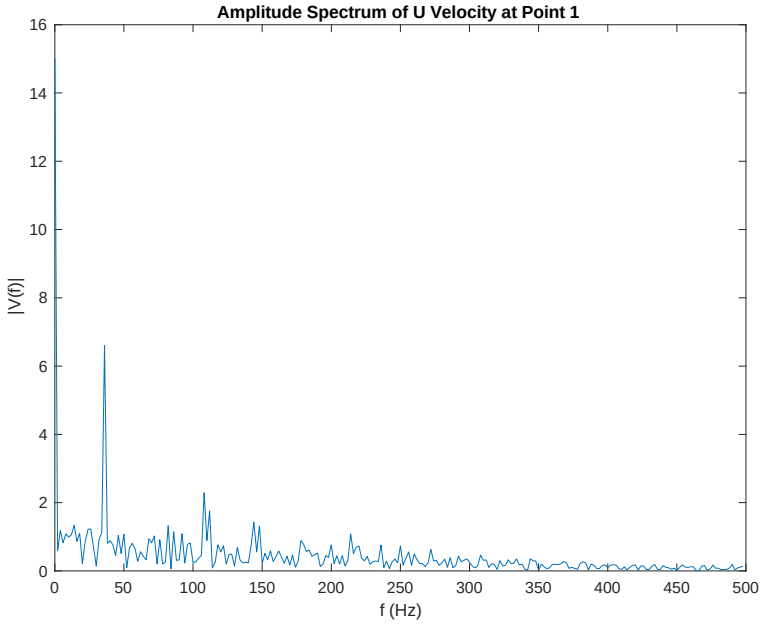

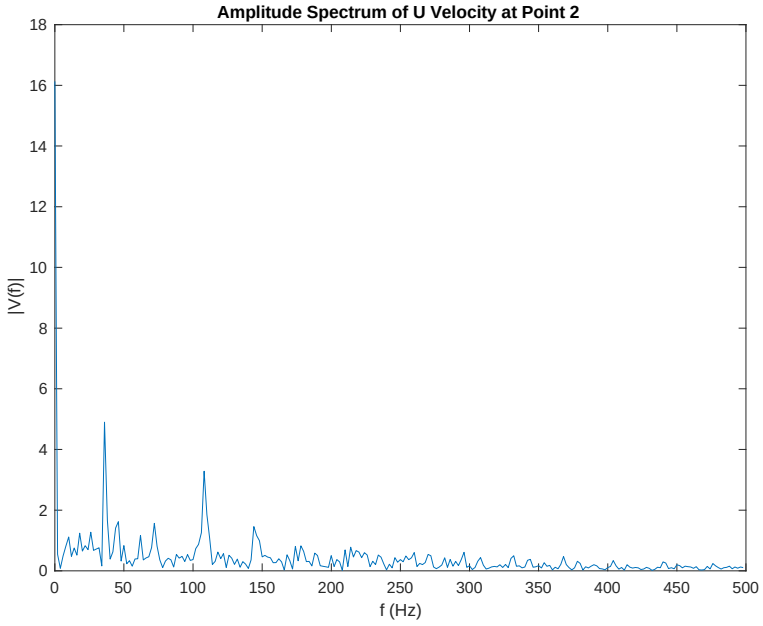

Inlet speed = 8.1625 m/s

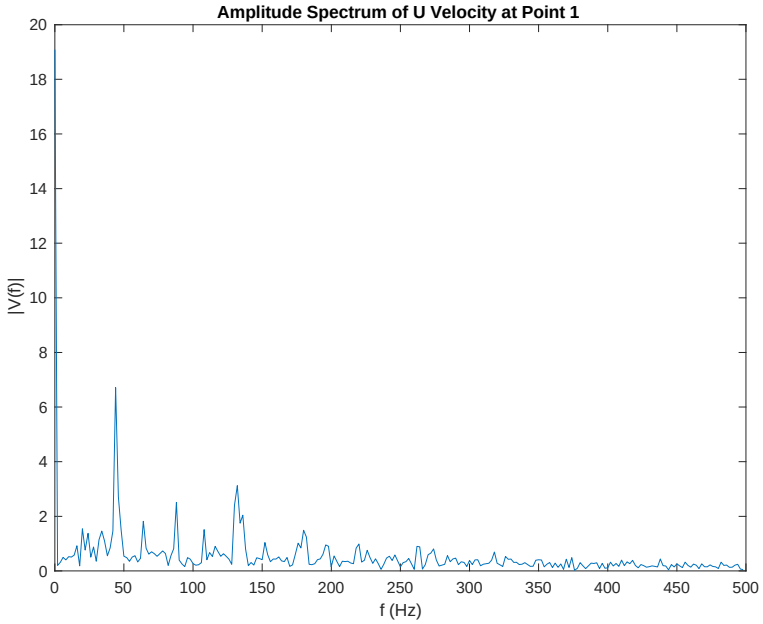

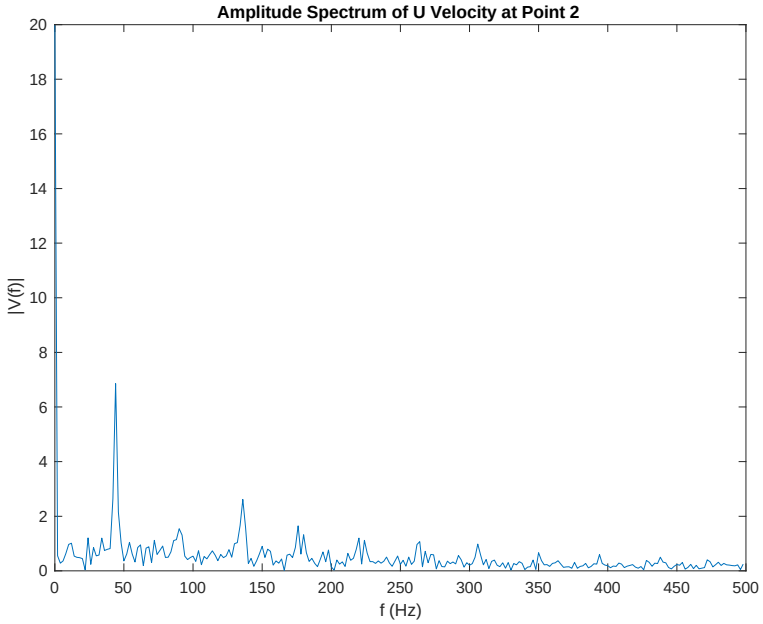

Inlet speed = 9.3455 m/s

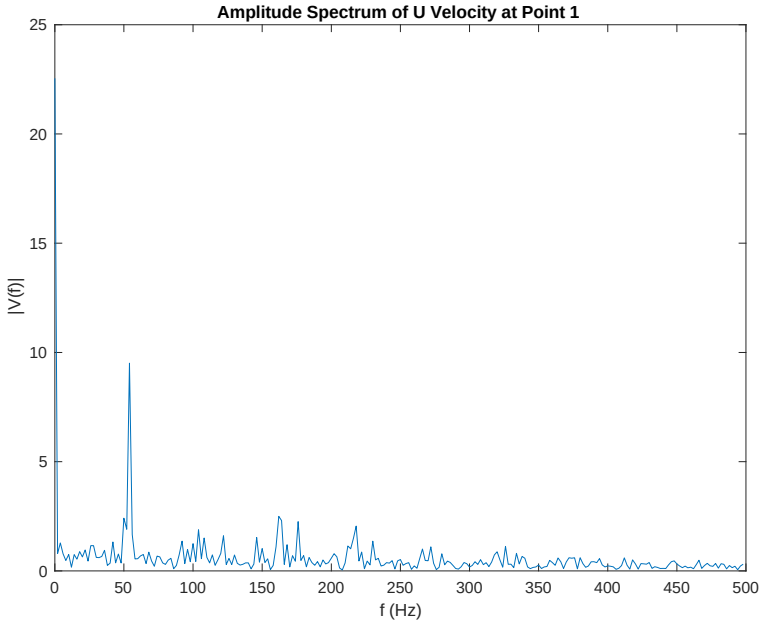

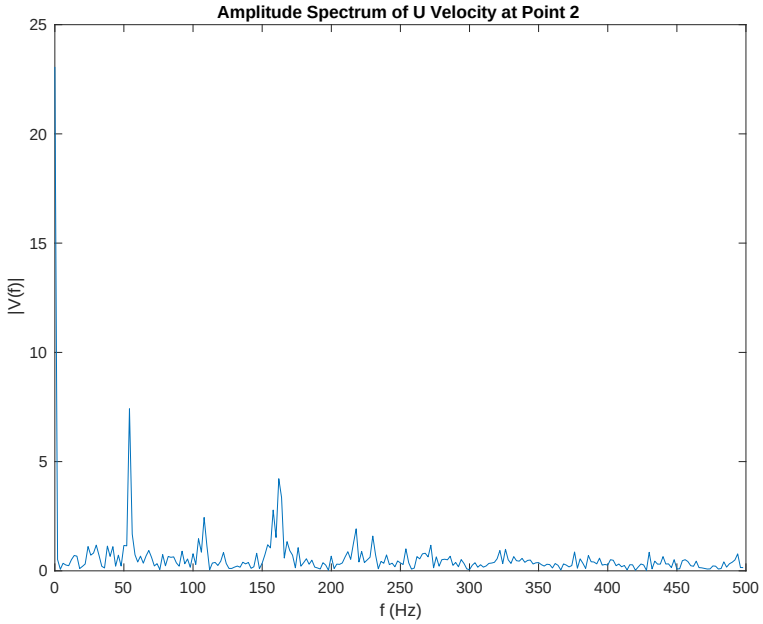

Inlet speed = 10.4989 m/s

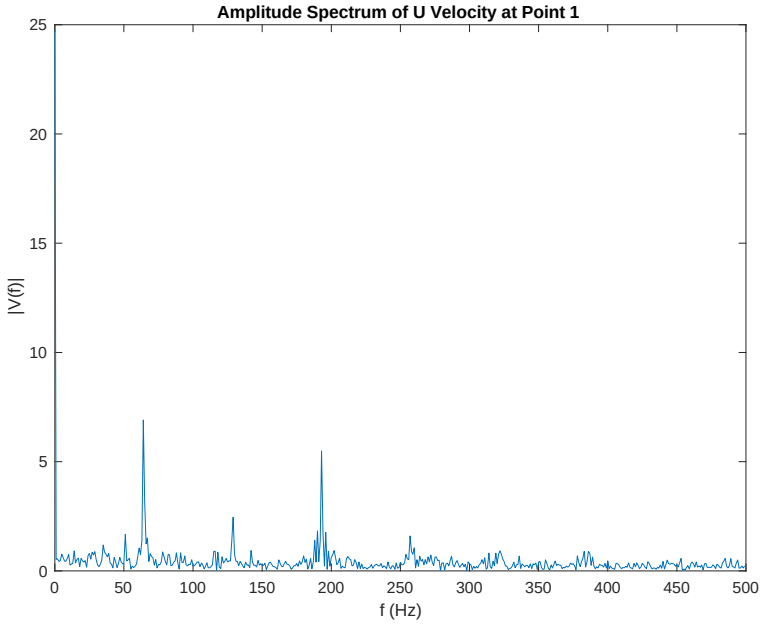

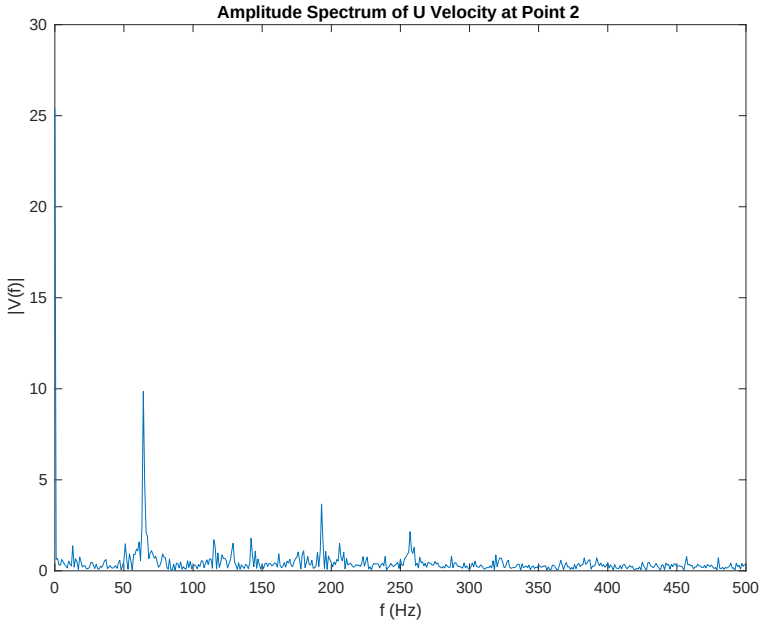

Inlet speed = 11.6819 m/s

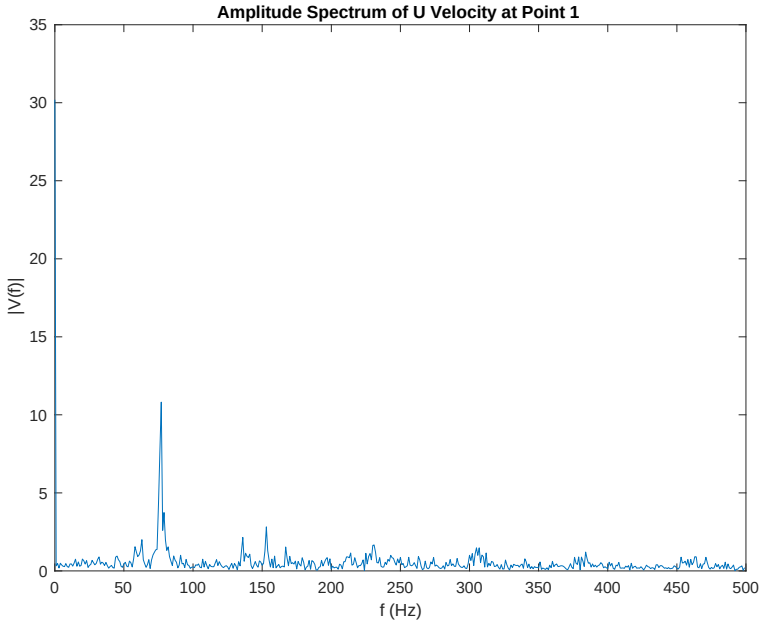

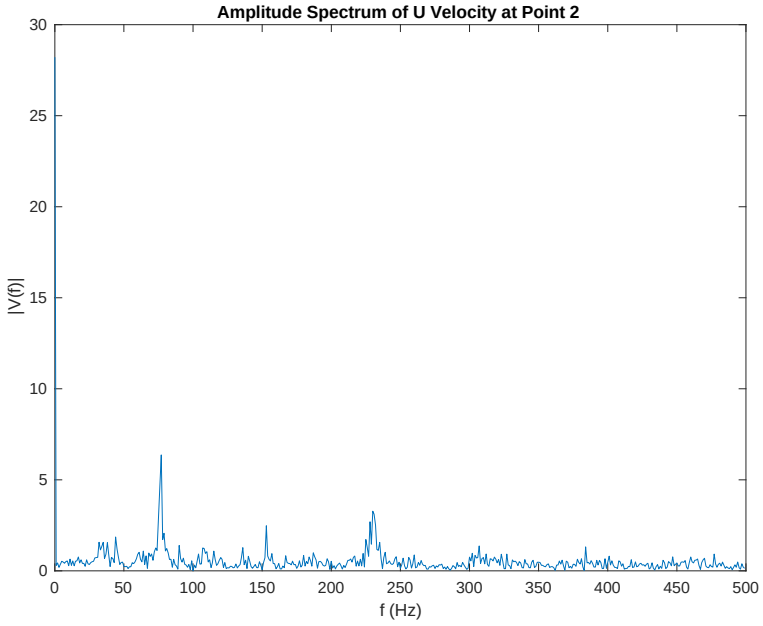

Inlet speed = 12.8353 m/s

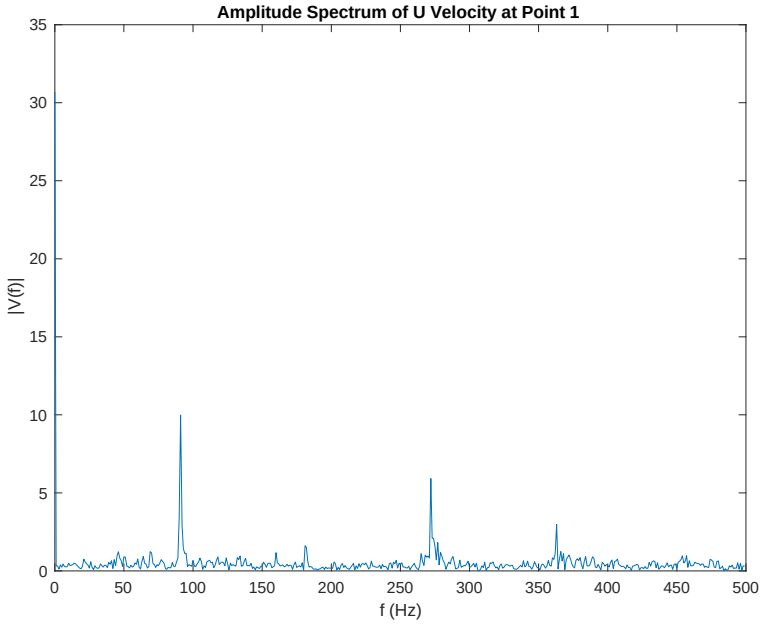

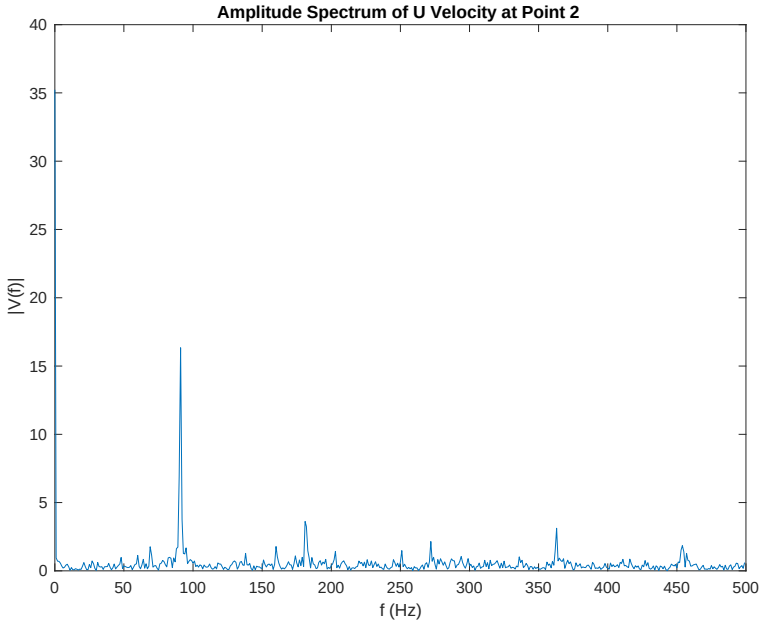

Inlet speed = 14.0182 m/s

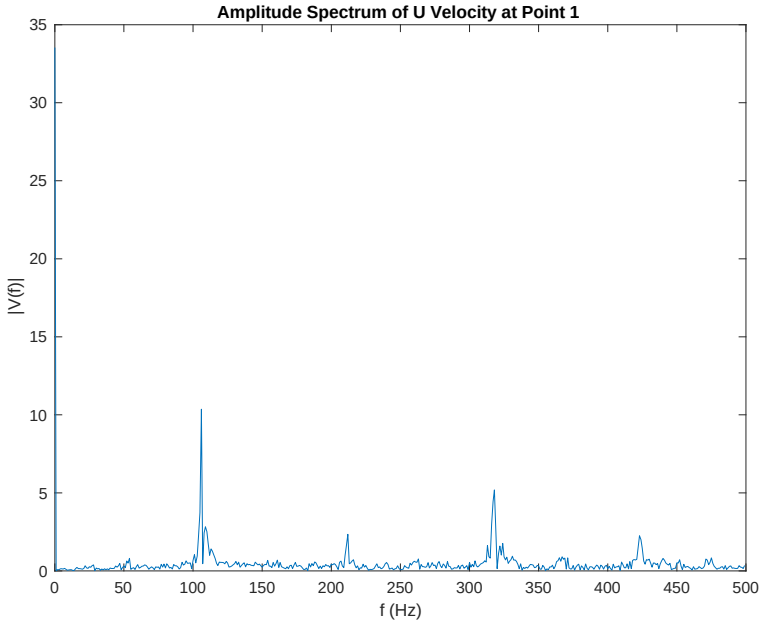

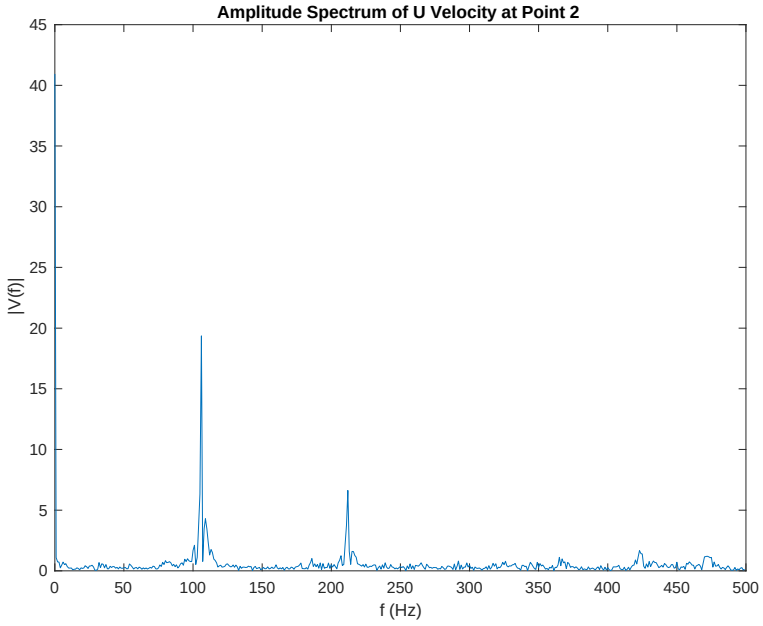

6. <u>Comparison of the experimental data and simulated oscillating frequency</u>

Mass Flow Rate (g/s)	Reynolds Number	Inlet Velocity (m/s)	Experimental Oscillating Frequency (Hz)	Simulated Oscillating Frequency (Hz)
0.79	4699	2.3364	146	7

1.18	7019	3.4898	210	14
1.58	9398	4.6727	284	22
1.97	11718	5.8261	352	28
2.37	14098	7.0091	414	36
2.76	16417	8.1625	466	44
3.16	18797	9.3455	514	54
3.55	21117	10.4989	560	64
3.95	23496	11.6819	605	77
4.34	25816	12.8353	644	91
4.74	28195	14.0182	680	106
5.13	30515	15.1716	684	122
	32180	16.0000		134
	34192	17.0000		143